REPORT NO. 85HV002
MAY 1985

PREPARED FOR MSFC
UNDER CONTRACT
NO. NAS8-36039

ANALYSIS AND CALCULATION OF MACROSEGREGATION IN A CASTING INGOT

FINAL REPORT

PREPARED BY
GENERAL ELECTRIC COMPANY
SPACE SYSTEMS DIVISION
HUNTSVILLE CENTER OPERATIONS
HUNTSVILLE, ALABAMA

GENERAL ELECTRIC

REPORT NO.: 85HV002
DATE: MAY 1985

MPS SOLIDIFICATION MODEL

FINAL REPORT
ANALYSIS AND CALCULATION OF MACROSEGREGATION IN A CASTING INGOT

PREPARED FOR MSFC
UNDER CONTRACT NAS8-36039

PREPARED BY:

Dr. David R. Poirier
Dept. of Metallurgical Engineering
University of Arizona

Anna L. Maples
Program Manager

APPROVED BY:

T. H. Thompson, Manager
Huntsville Operations

J. W. Neiers, Manager,
Data Systems and Technology

TABLE OF CONTENTS

TABLE OF CONTENTS (Continued)

LIST OF ILLUSTRATIONS

LIST OF ILLUSTRATIONS (Continued)

LIST OF ILLUSTRATIONS (Continued)

LIST OF TABLES

SECTION 1
INTRODUCTION

This report describes work performed under Contract NAS8-36039 on several existing solidification models for which computer codes and documentation were developed under Contract, NAS8-33573. The models describe the solidification of alloys in which there is a time-varying zone of coexisting solid and liquid phases; i.e., the S/L zone. The primary purpose of the models is to calculate macrosegregation in a casting or ingot which results from flow of interdendritic liquid in this S/L zone during solidification. The flow, driven by solidification contractions and by gravity acting on density gradients in the interdendritic liquid, is modeled as flow through a porous medium. In Model 1, the "steady-state model," the heat flow characteristics are those of steady-state solidification; i.e., the S/L zone is of constant width and it moves at a constant velocity relative to the mold (1). In Model 2, the "unsteady-state model," the width and rate of movement of the S/L zone are allowed to vary with time as it moves through the ingot (2). Each of these models exists in two versions. Models 1 and 2 are applicable to binary alloys; models 1M and 2M are applicable to multicomponent alloys (3).

Several enhancements to the models and their associated data bases are described here. Two new multicomponent alloys, MAR-M246(Hf) and PWA 1480 (Alloy 454), were added to the data base. The development of the data for these alloys is described in Appendices A and B; sample results are in Section 2. A new graphical output selection has been added to all four programs to allow display of the region in the S/L zone where gas-caused porosity may develop. This feature is described in Section 3 and in Appendix C. All programs developed or modified under contracts NAS8-33573 and NAS8-36039 were installed on a VAX* computer at Marshall Space Flight Center. The operating and maintenance procedures for this installation of the materials processing programs are in Section 4.

---

*VAX is a trademark of Digital Equipment Corporation

SECTION 2
NEW MULTICOMPONENT ALLOYS

The original solidification models were designed for binary alloys (1,2). They operate from a data base containing all input data for each alloy, so that applying the models to a new binary alloy just requires an addition to the data base. Under a previous contract, parallel versions of the steady-state and unsteady-state models were developed for multicomponent alloys. The change from binary to multicomponent alloys required substantial model changes (3). The multicomponent models also operate from a data base, so that applying the model to the two new alloys, MAR-M246(Hf) and PWA 1480, only required that the alloy data be developed and included in the data base. The data were developed as shown in Appendices A and B by Dr. Poirier of the University of Arizona. These data include the liquid and solid metal densities and a local approximation to the phase diagram. Due to the limited time available under this contract, data were estimated by a purely analytical process which used the published properties of related alloys and pure metals, rather than determined empirically. The multicomponent data base now contains three alloys; the alloy selection page of the interactive model input is shown below:

```
1  MAR-M246
2  MAR-M246(Hf)
3  PWA 1480 (ALLOY 454)


ENTER ALLOY NUMBER
```

Sample cases from the steady-state and the unsteady-state models for both new alloys are in the following subsections.

2.1 MAR-M246(Hf)

The properties for MAR-M246(Hf) are shown in Fig. 2.1. Steady-state and unsteady-state cases have been run for the same input conditions as the MAR-M246 cases in Sections 3.4.3 and 3.4.4 of Ref. 3. The graphical output from those cases follows.

REFERENCE TEMPERATURE	1.389E+03 DEG C
EUTECTIC TEMPERATURE	1.230E+03 DEG C
SOLID DENSITY	7.820E+00 GM/CM**3
REFERENCE DENSITY	7.820E+00 GM/CM**3
SOLID EUTECTIC DENSITY	8.050E+00 GM/CM**3
DENSITY/TEMPERATURE DEPENDENCE	-1.250E-03 GM/CM**3 / DEG C
VISCOSITY	4.000E-02 GM/(CM*SEC)
SURFACE TENSION	1.700E+03 DYNES/CM

COMPONENT	COMPOSITION (WEIGHT PERCENT)	EQUILIBRIUM PARTITION RATIO	TEMPERATURE/ COMPOSITION DEPENDENCE	DENSITY/ COMPOSITION DEPENDENCE	HYDROGEN INTERACTION COEFFICIENT
CR	9.000E+00	9.000E-01	-2.200E+00	-1.300E-02	3.600E-03
CO	1.000E+01	1.100E+00	0.000E+00	1.000E-03	3.100E-03
AL	5.500E+00	1.100E+00	-3.200E+00	-1.100E-01	1.400E-02
TI	1.500E+00	9.500E-01	-7.700E+00	-3.500E-02	1.300E-02
W	1.000E+01	1.200E+00	3.500E+00	4.200E-02	1.100E-02
MO	2.500E+00	6.500E-01	-1.000E+00	3.300E-02	1.100E-02
TA	1.500E+00	9.700E-01	-2.500E+00	3.500E-02	1.100E-02
C	1.500E-01	2.500E-01	-6.100E+01	-7.200E-01	6.500E-02
HF	1.500E+00	2.300E-01	-1.040E+01	5.200E-02	1.100E-02

Figure 2.1. Properties of MAR-M246(Hf)

2.1.1 STEADY-STATE EXAMPLE

Graphs are shown from the steady-state model operating on MAR-M246(Hf) for the same solidification conditions as in the MAR-M246 case in Ref. 3. Fig. 2.2 is a plot of volume fraction liquid across the S/L zone. Fig. 2.3 shows the interdendritic fluid flow. Fig. 2.4 shows the final local average weight percent of each element. The maximum fluid velocity in this case is only about one-fourth the maximum velocity in the MAR-M246 case. As in the case of MAR-M246, the vectors are all vertical and downward, and there is no macrosegregation.

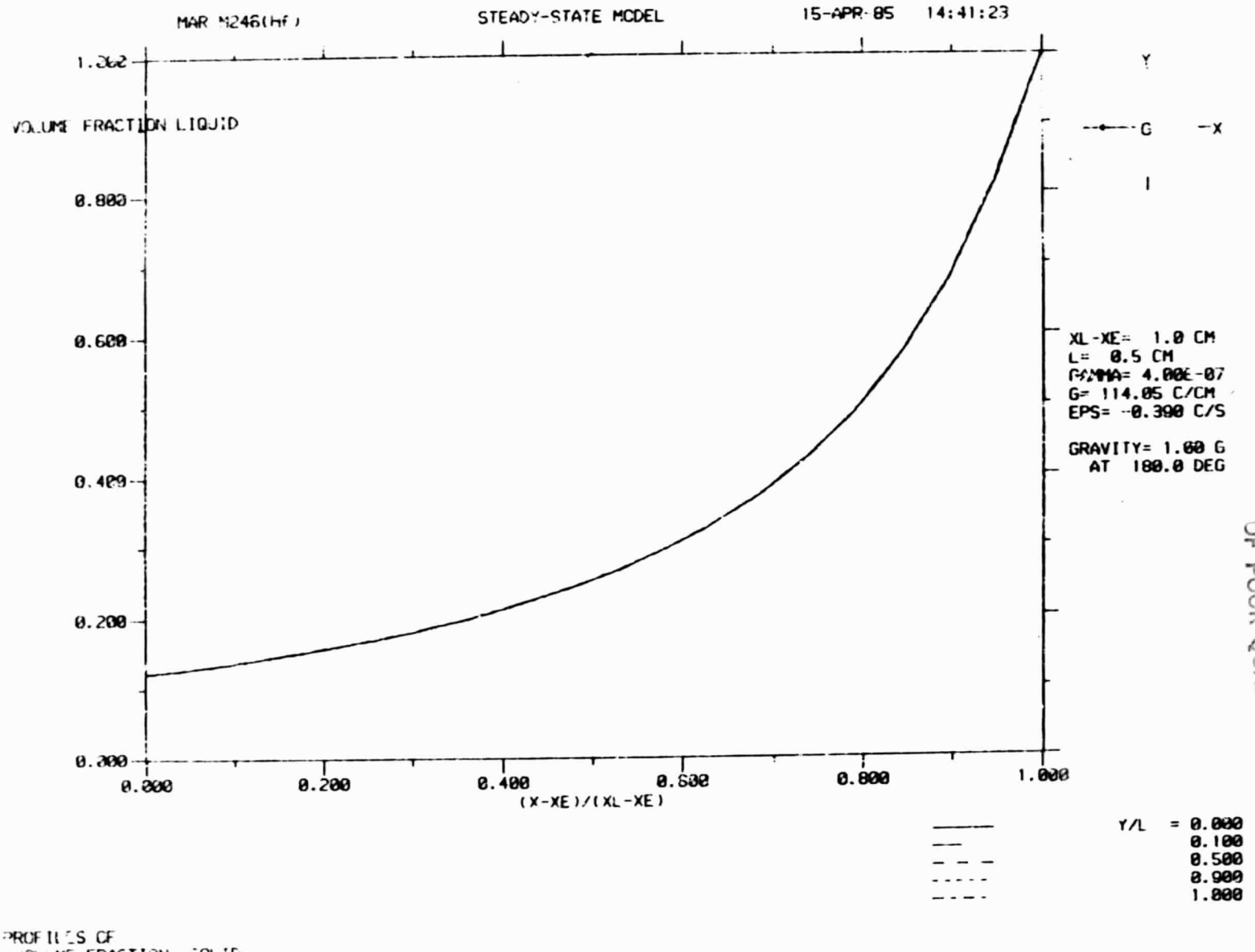

Figure 2.2. Volume Fraction Liquid Across the S/L Zone

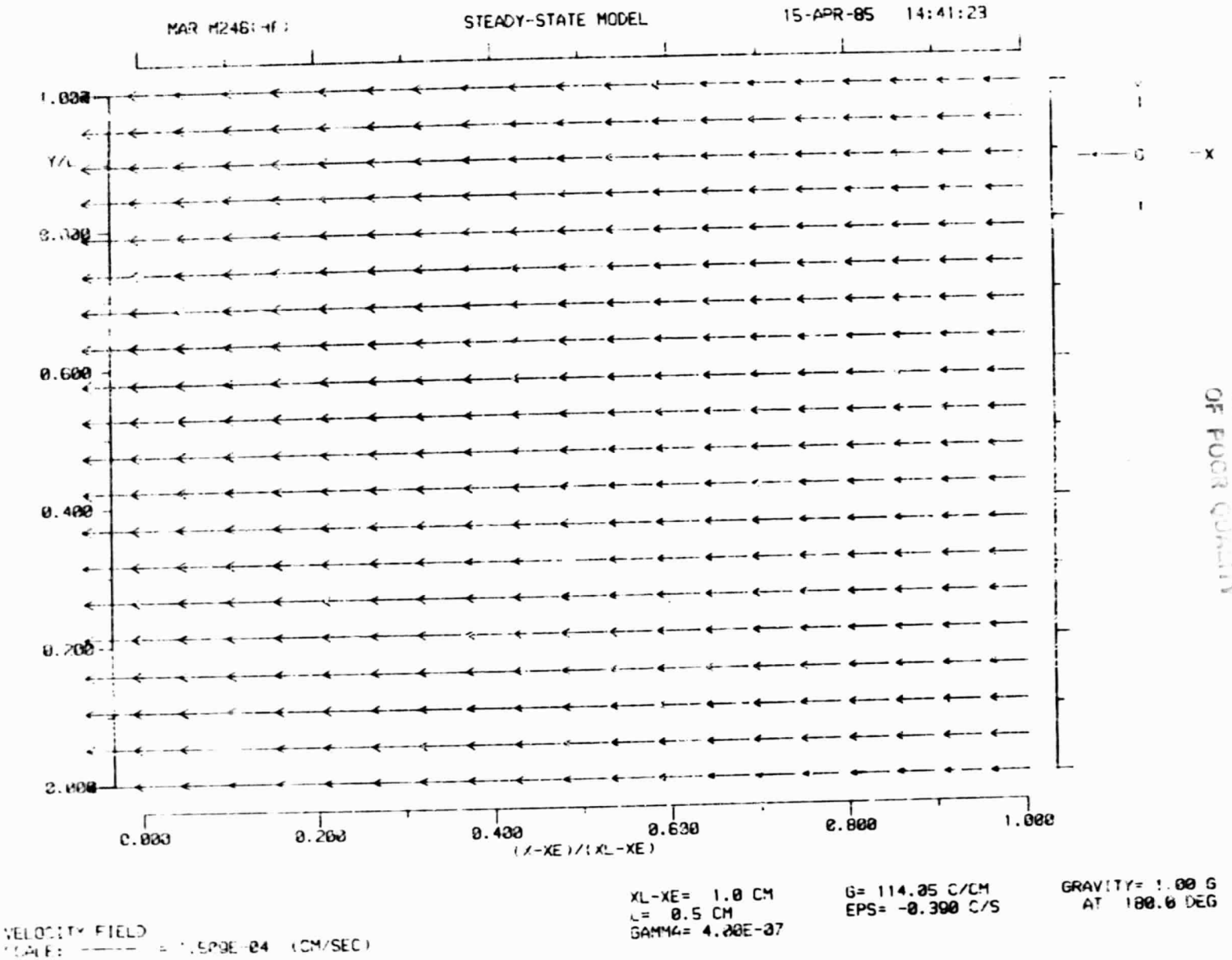

Figure 2.3. Interdendritic Fluid Flow

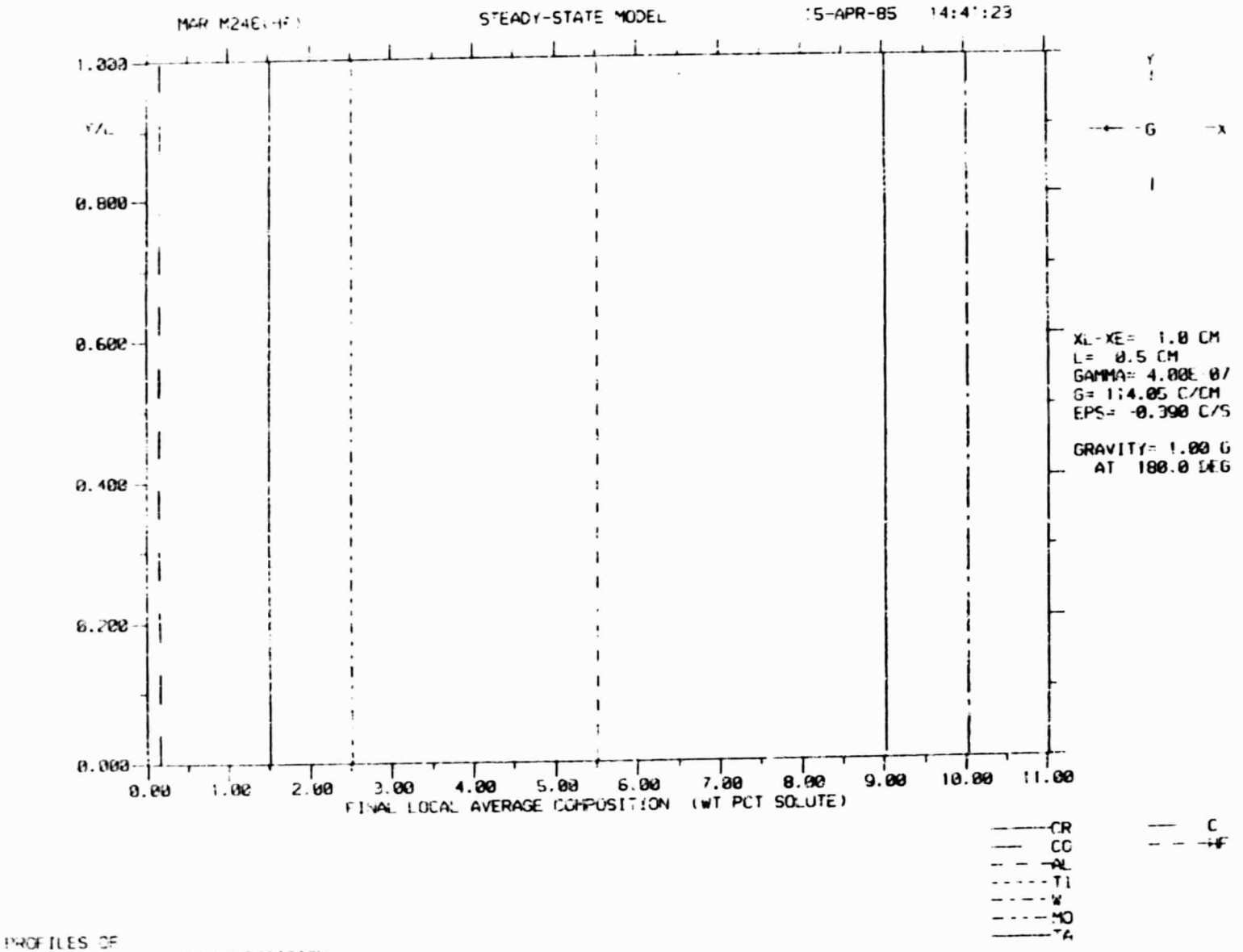

Figure 2.4. Final Local Average Weight Percent of Each Element

2.1.2 UNSTEADY-STATE EXAMPLE

The output shown here is directly comparable to the output for MAR-M246 shown in Ref. 3. The first two plots (Fig. 2.5 and 2.6) show the interdendritic fluid flow in the S/L zone and contours of the weight percent of chromium in the final solid when the solidus has progressed to 3 cm from the chill and the liquidus is at 4 cm from the chill. The remaining plots (Fig. 2.7 through 2.15) show the vertical profile of each element in the solidified casting. Because the solidification is vertical, there is essentially no segregation except for the inverse segregation near the chill.

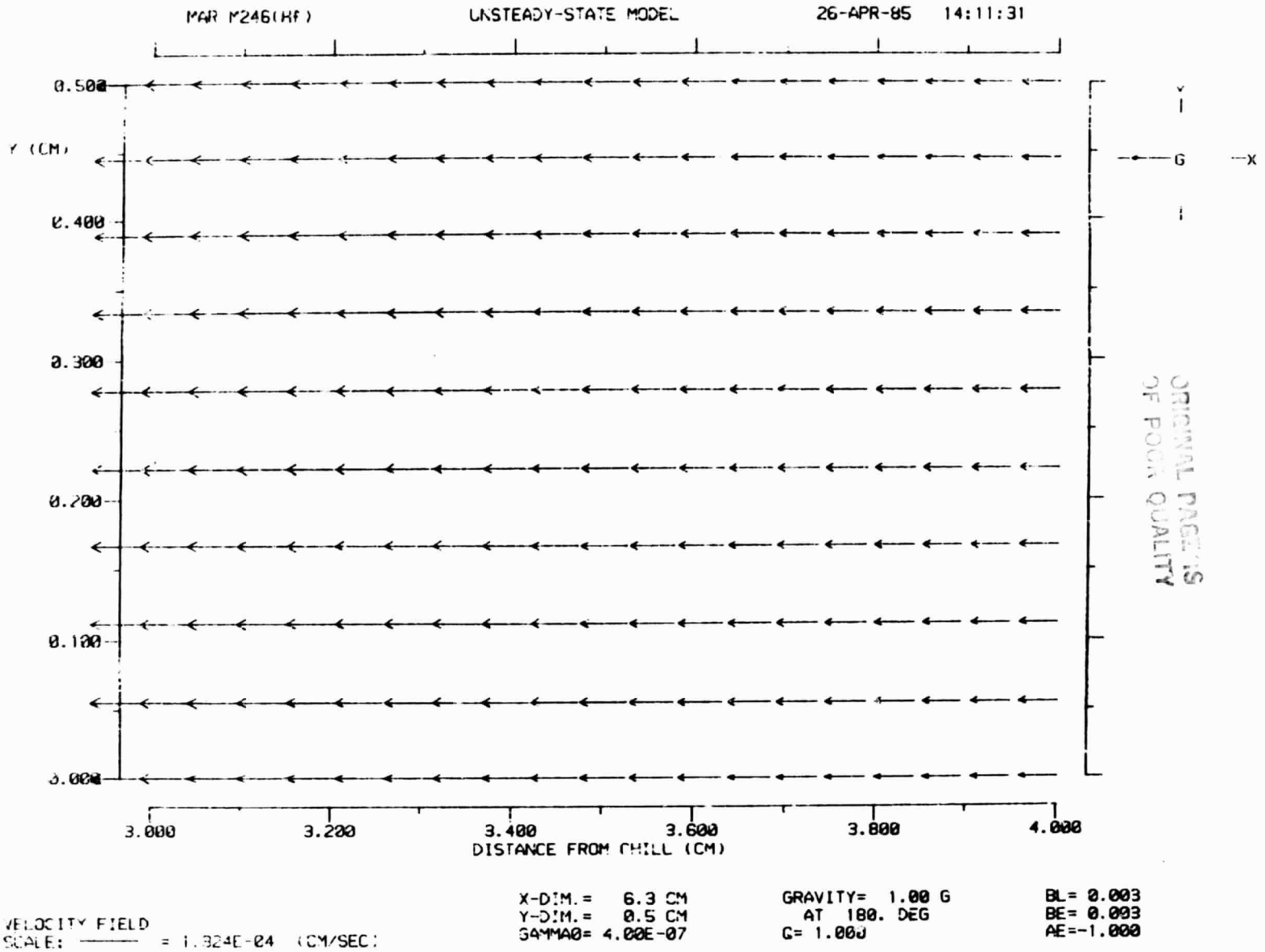

Figure 2.5. Interdendritic Fluid Flow in the S/L Zone (Plot 1)

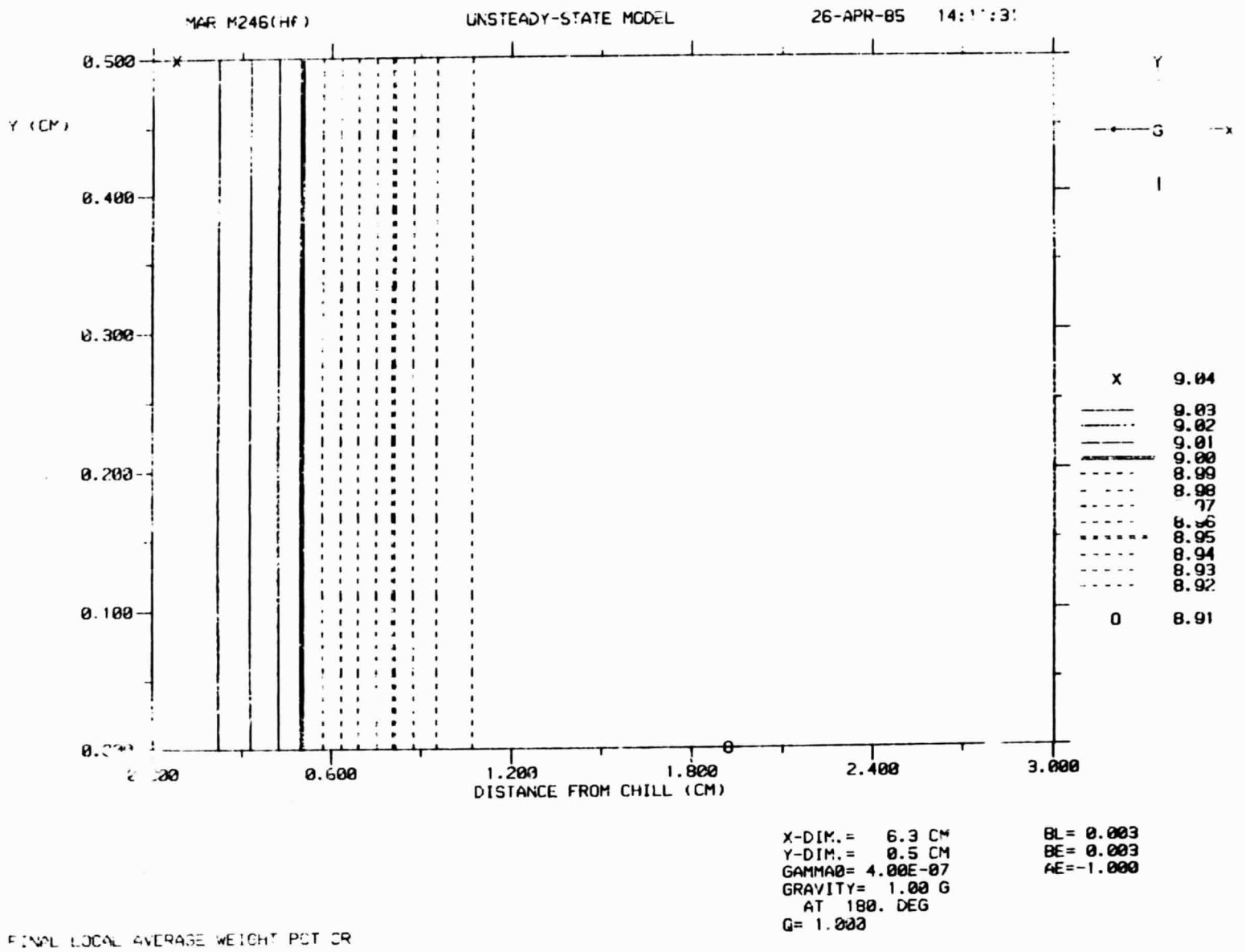

Figure 2.6. Contours of the Weight Percent of Chromium (Plot 2)

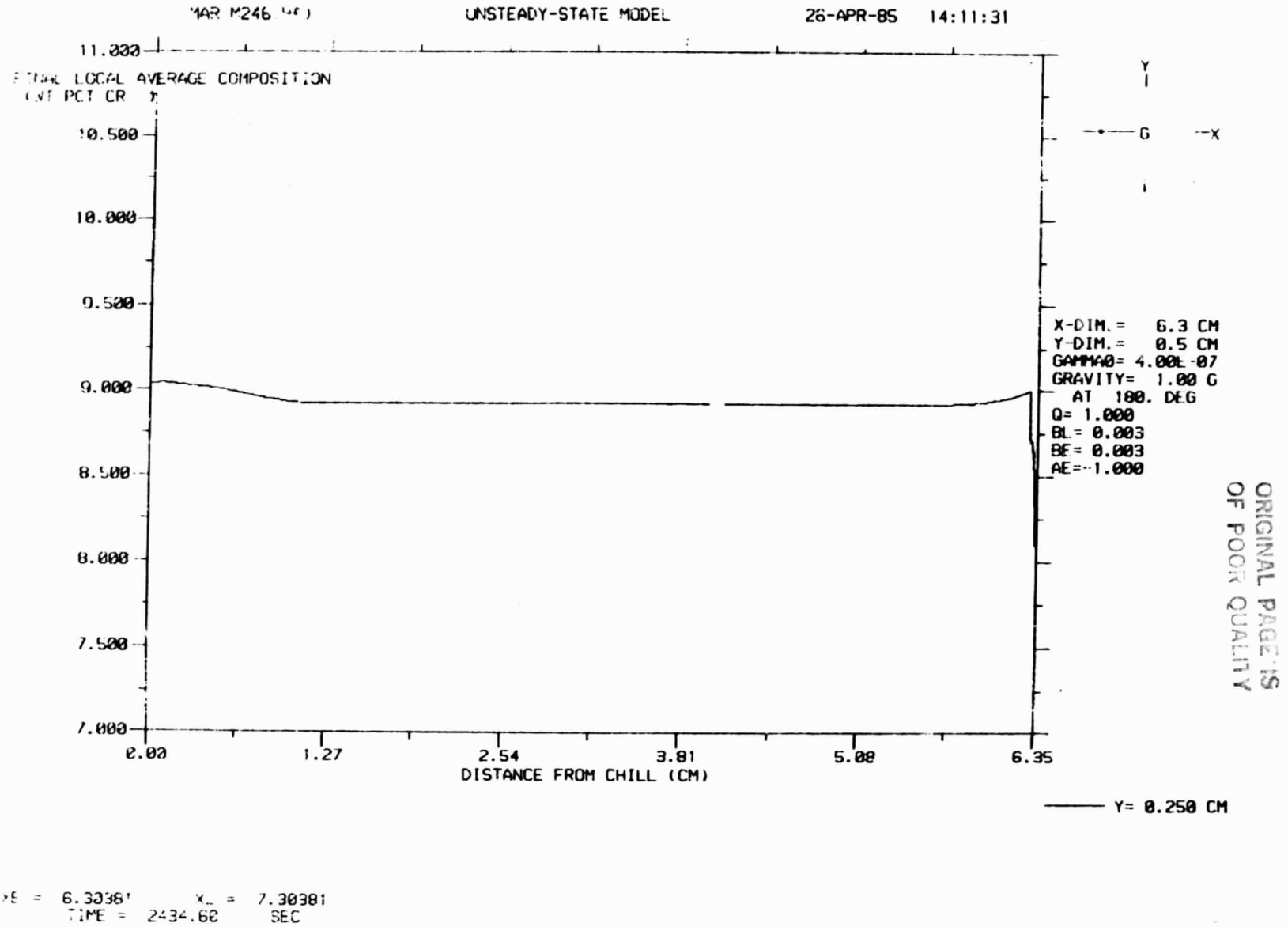

Figure 2.7. Vertical Profile of Each Element in Solidified Casting (Plot 3)

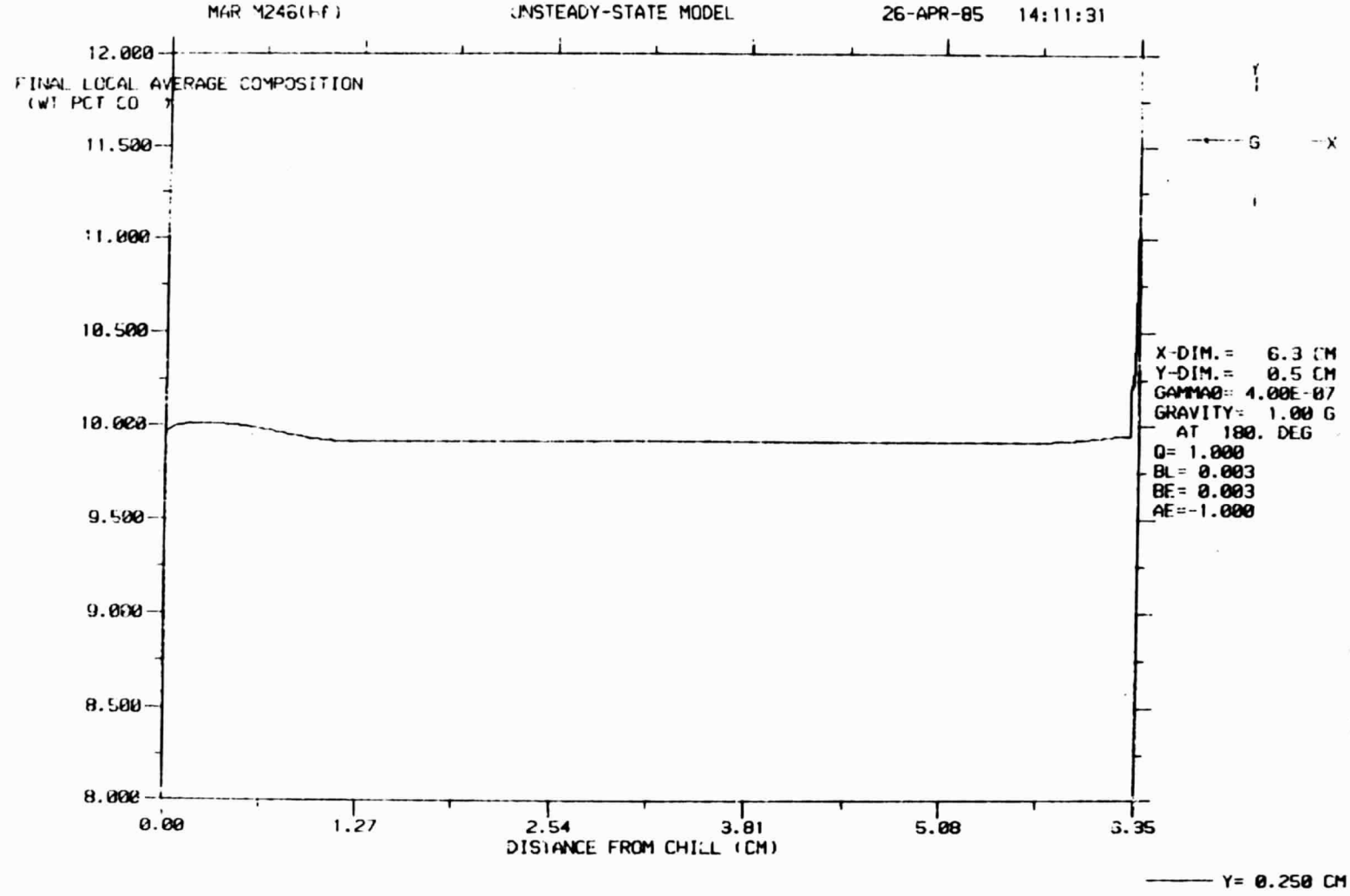

XE = 6.30381 XL = 7.30381
TIME = 2434.60 SEC

Figure 2.8. Vertical Profile of Each Element in Solidified Casting (Plot 4)

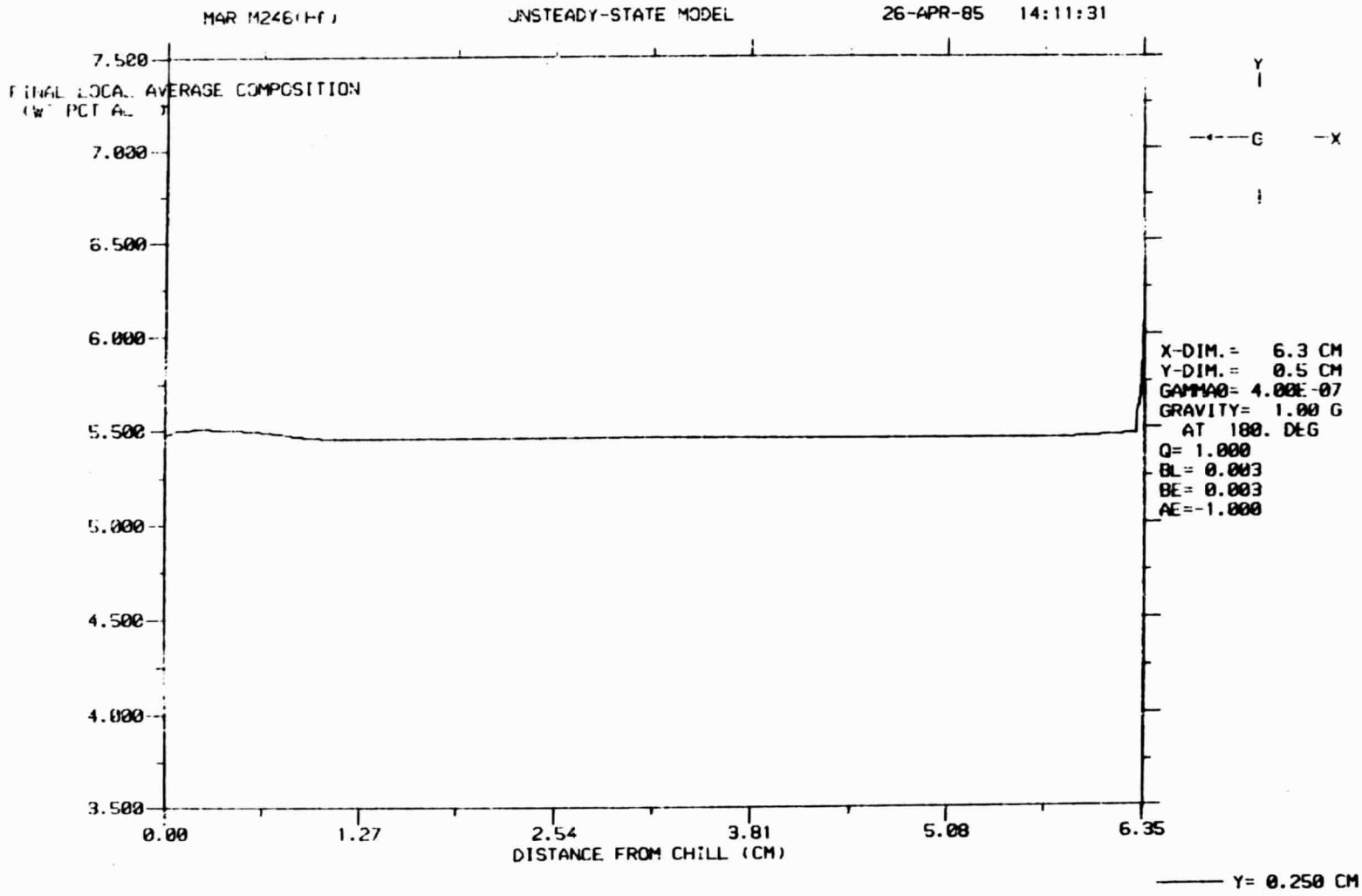

Figure 2.9. Vertical Profile of Each Element in Solidified Casting (Plot 5)

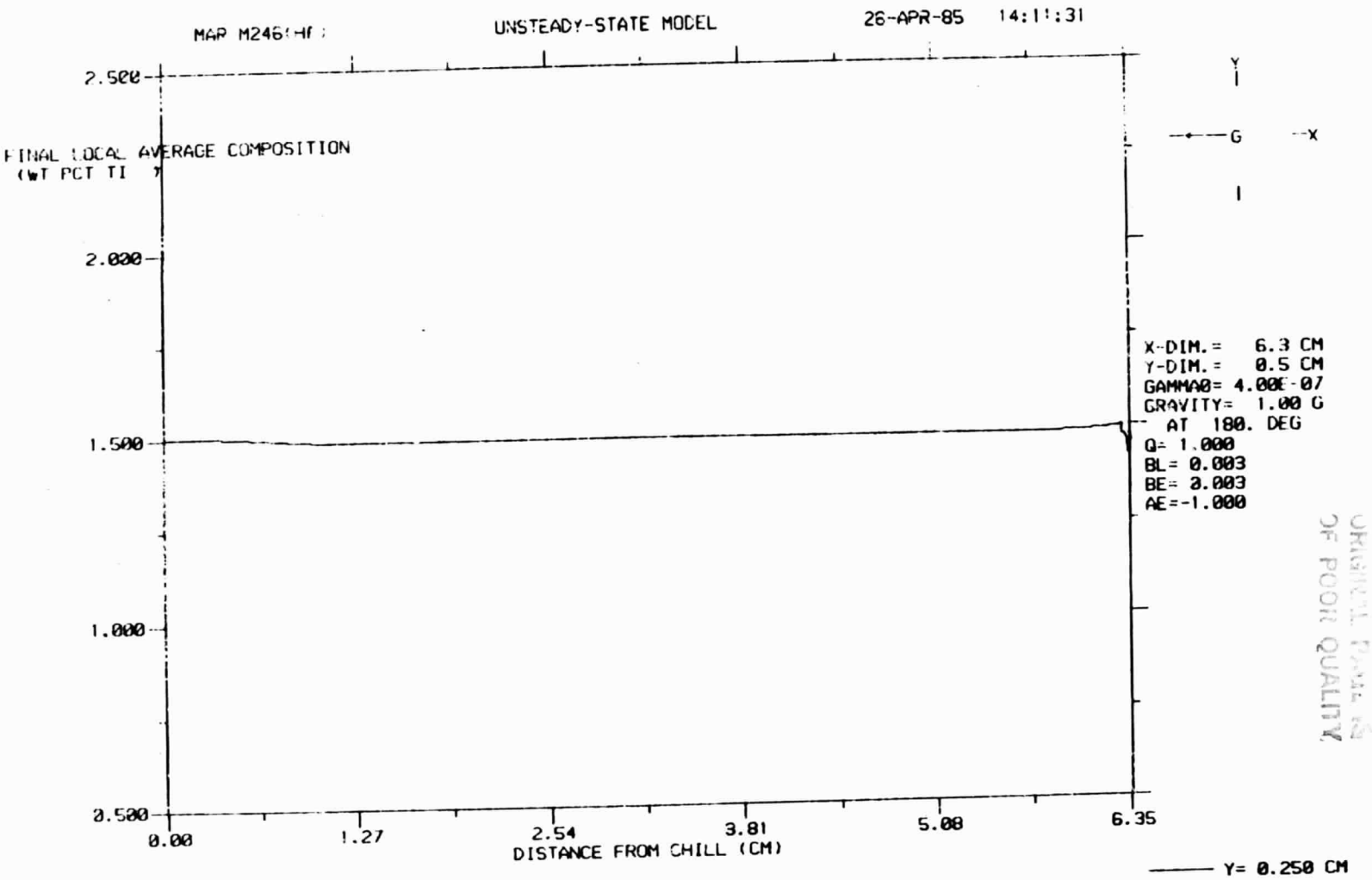

Figure 2.10. Vertical Profile of Each Element in Solidified Casting (Plot 6)

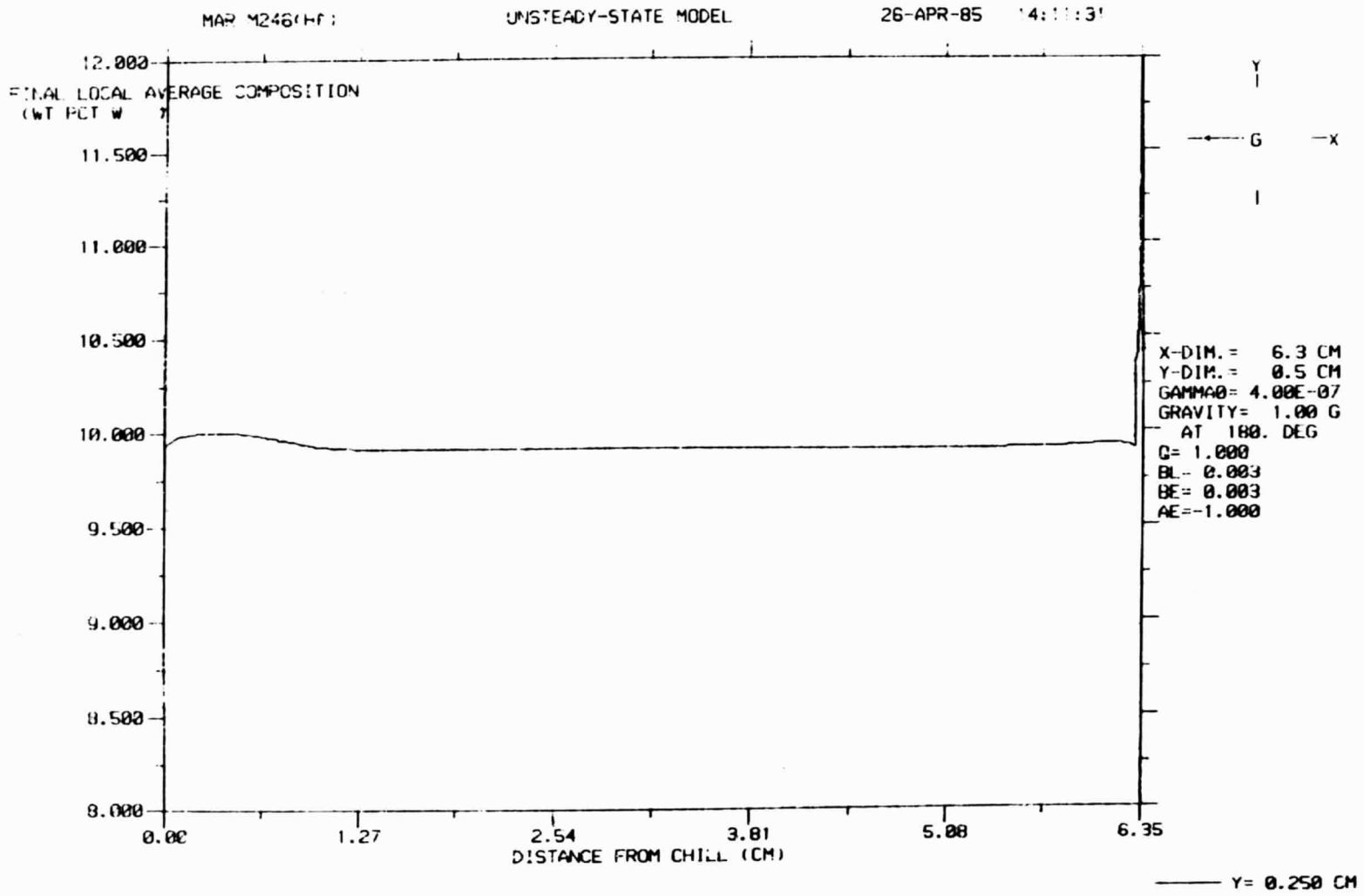

Figure 2.11. Vertical Profile of Each Element in Solidified Casting (Plot 7)

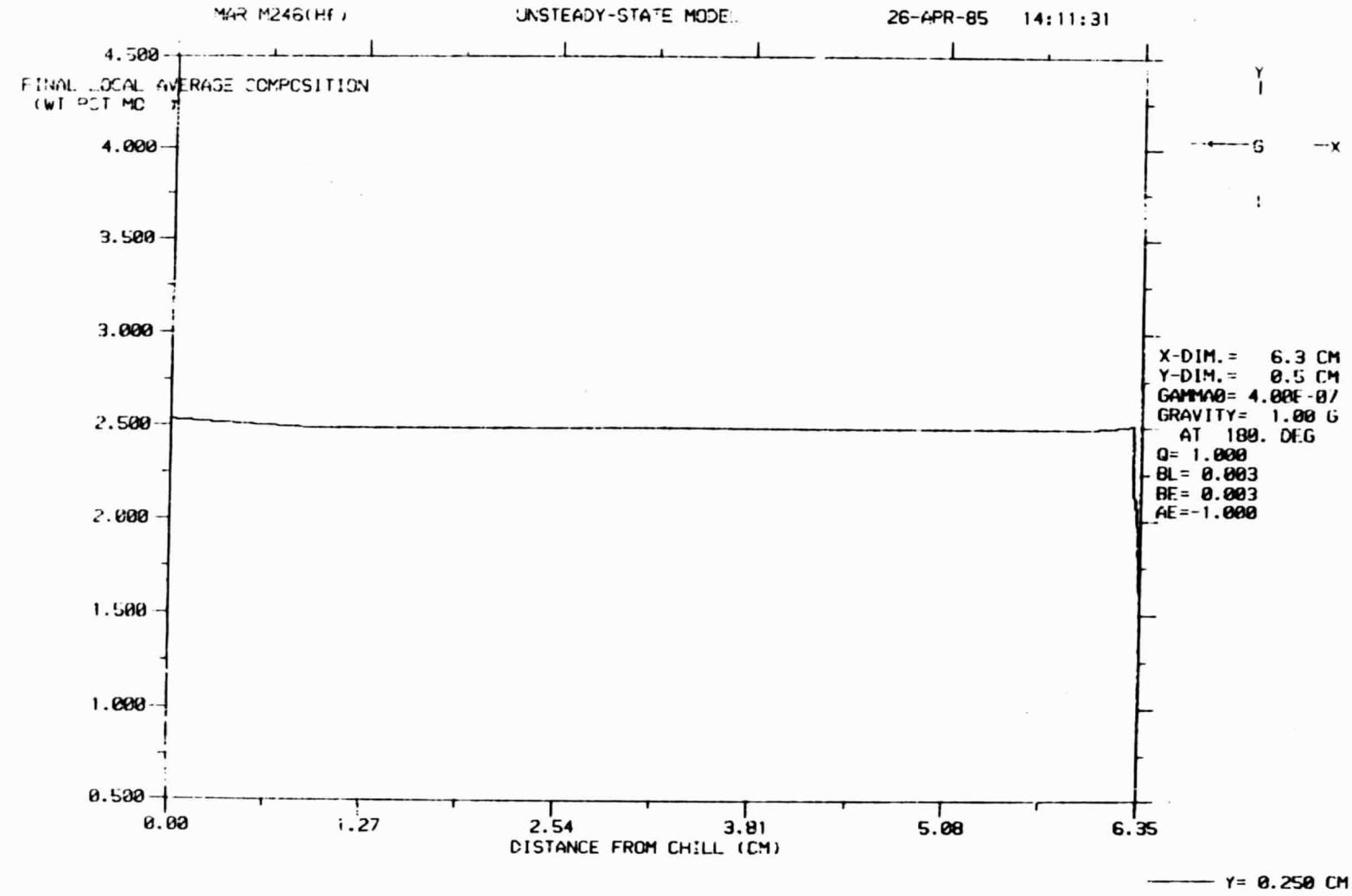

XE = 6.3038; XL = 7.3038;
TIME = 2434.60 SEC

Figure 2.12. Vertical Profile of Each Element in Solidified Casting (Plot 8)

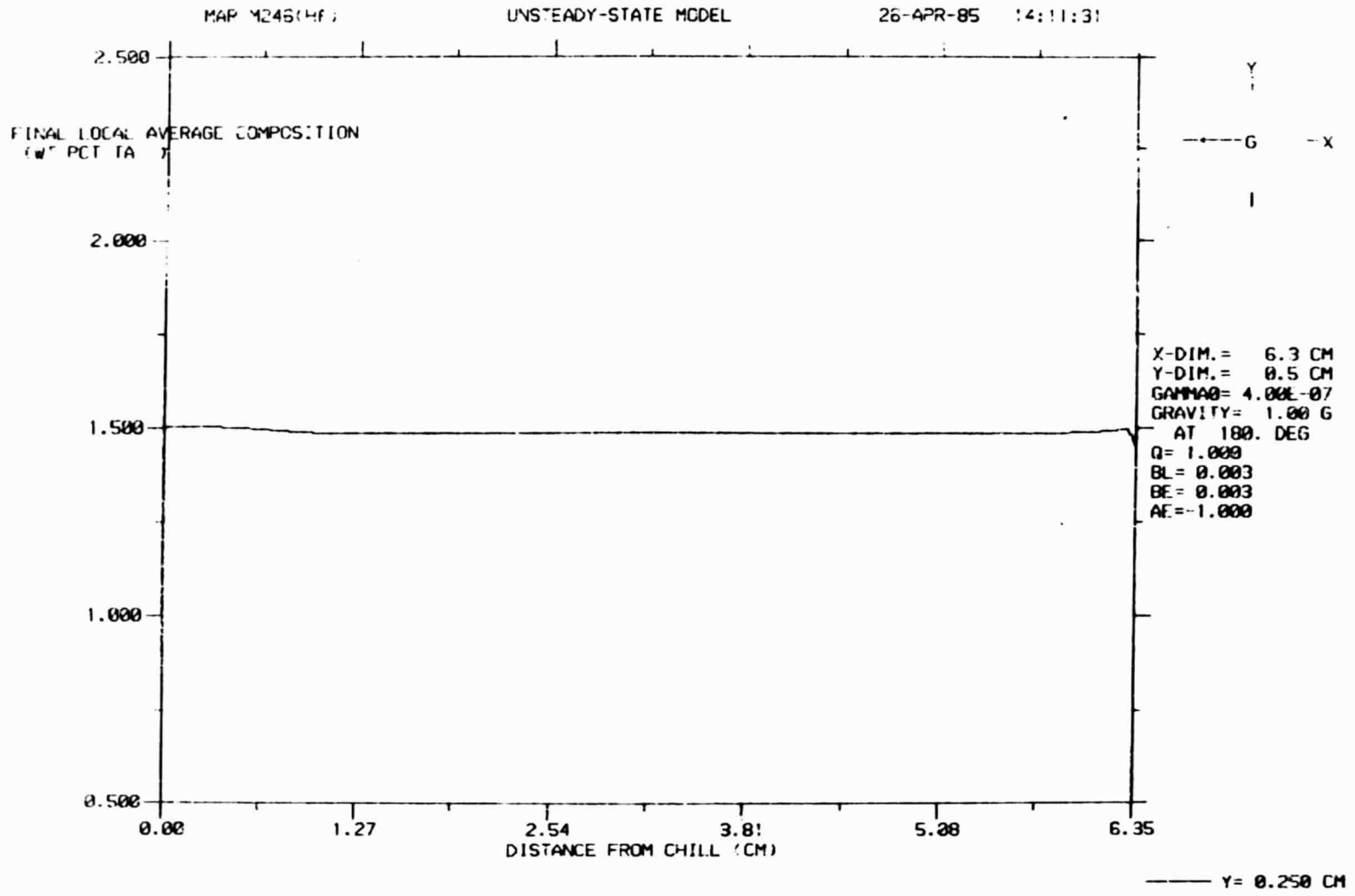

XE = 6.30381 XL = 7.30381
TIME = 2434.60 SEC

Figure 2.13. Vertical Profile of Each Element in Solidified Casting (Plot 9)

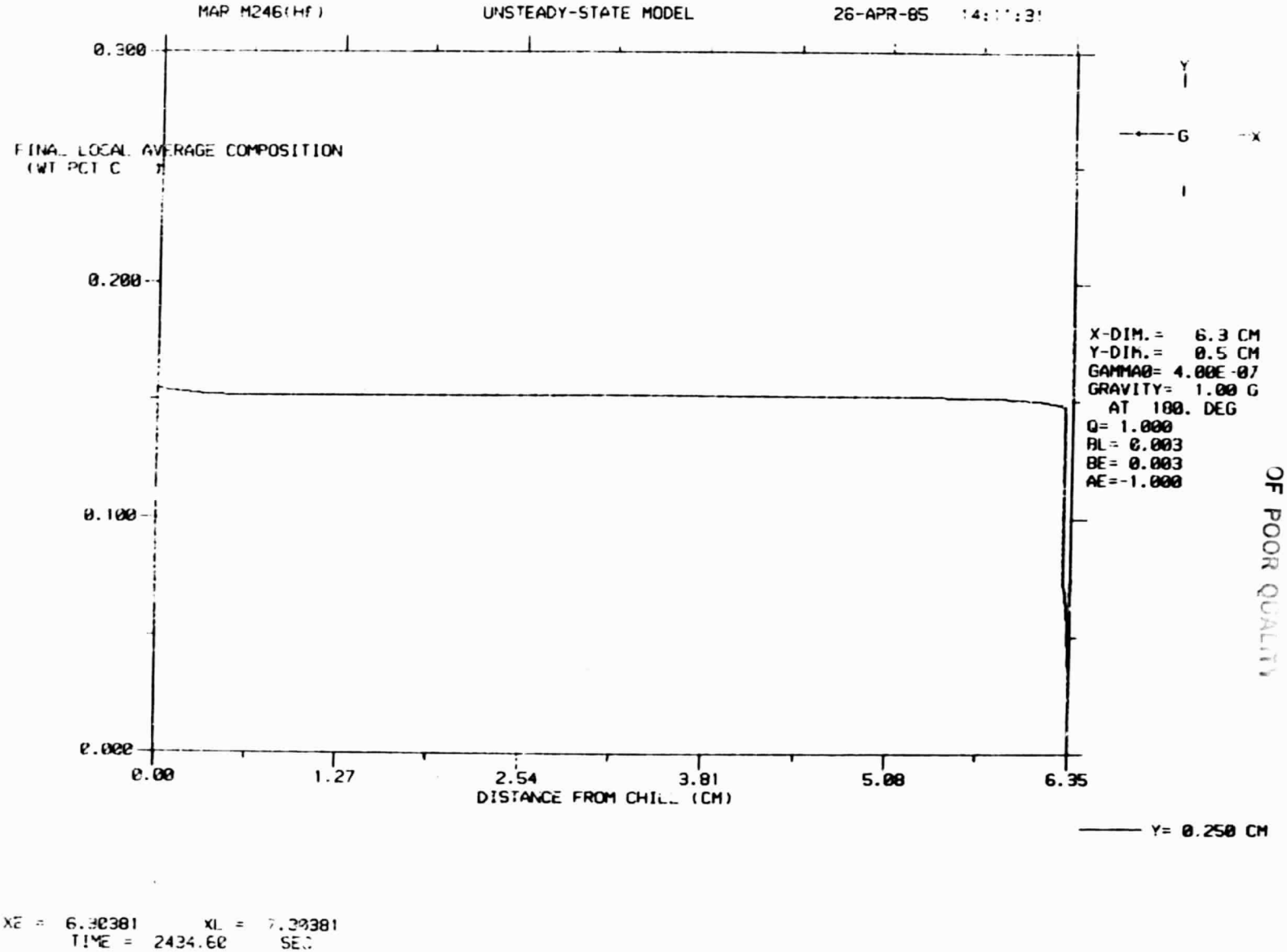

Figure 2.14. Vertical Profile of Each Element in Solidified Casting (Plot 10)

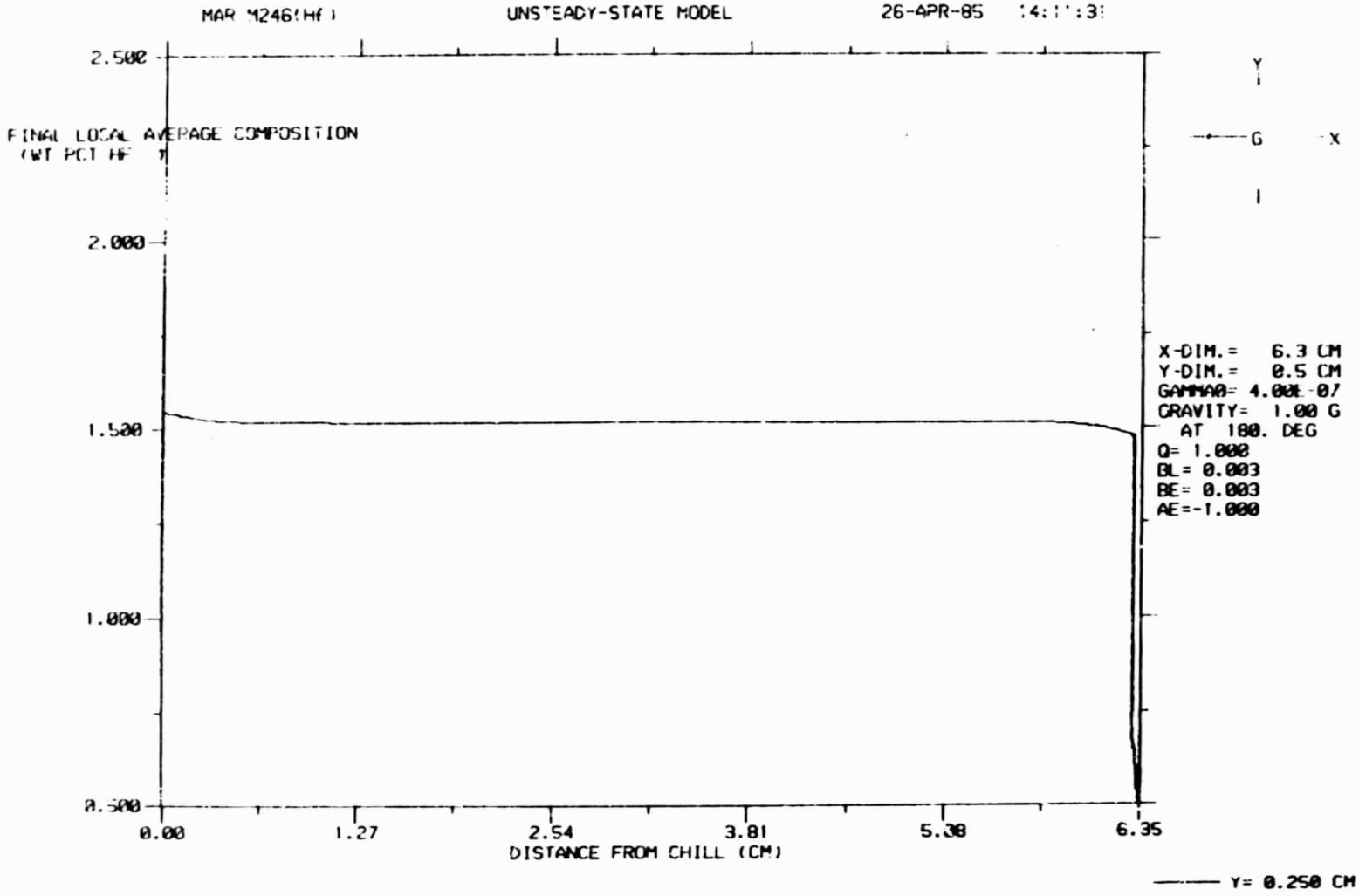

Figure 2.15. Vertical Profile of Each Element in Solidified Casting (Plot 11)

2.2 PWA 1480 (ALLOY 454)

The properties for PWA 1480 are shown in Fig. 2.16. Steady-state and unsteady-state cases have been run for the same input conditions as the MAR-M246 cases in Sections 3.4.3 and 3.4.4 of Ref. 3. The graphical output from those cases are shown in Sections 2.2.1 and 2.2.2.

REFERENCE TEMPERATURE	1.460E+03	DEG C
EUTECTIC TEMPERATURE	1.200E+03	DEG C
SOLID DENSITY	7.770E+00	GM/CM**3
REFERENCE DENSITY	7.720E+00	GM/CM**3
SOLID EUTECTIC DENSITY	7.860E+00	GM/CM**3
DENSITY/TEMPERATURE DEPENDENCE	-1.250E-03	GM/CM**3 / DEG C
VISCOSITY	4.000E-02	GM/(CM*SEC)
SURFACE TENSION	1.710E+03	DYNES/CM

COMPONENT	COMPOSITION (WEIGHT PERCENT)	EQUILIBRIUM PARTITION RATIO	TEMPERATURE/ COMPOSITION DEPENDENCE	DENSITY/ COMPOSITION DEPENDENCE	HYDROGEN INTERACTION COEFFICIENT
CR	1.000E+01	9.000E-01	-2.200E+00	-1.300E-02	3.600E-03
CO	5.000E+00	1.100E+00	0.000E+00	1.000E-03	3.100E-03
AL	5.000E+00	9.500E-01	-3.200E+00	-1.100E-01	1.400E-02
TI	1.500E+00	5.500E-01	-7.700E+00	-3.500E-02	1.300E-02
W	4.000E+00	1.200E+00	3.500E+00	4.200E-02	1.100E-02
TA	1.200E+01	7.000E-01	-2.500E+00	3.500E-02	1.100E-02

Figure 2.16. Properties of PWA 1480 (Alloy 454)

2.2.1 STEADY-STATE EXAMPLE

This example is directly comparable to the steady-state example in Section 2.1 and to the MAR-M246 example in Ref. 3. The same three plots are shown (Fig. 2.17, 2.18, and 2.19). In the case of PWA 1480, the velocity vectors near the solidus are vertical and point upward indicating some expansion of the final material to solidify. In this case, the liquid eutectic has a density of 8.12 gm./cc while the solid eutectic has a density of 8.05 gm./cc. The maximum velocity occurs in the upward flowing material. With vertical, steady-state solidification, no macrosegregation is predicted.

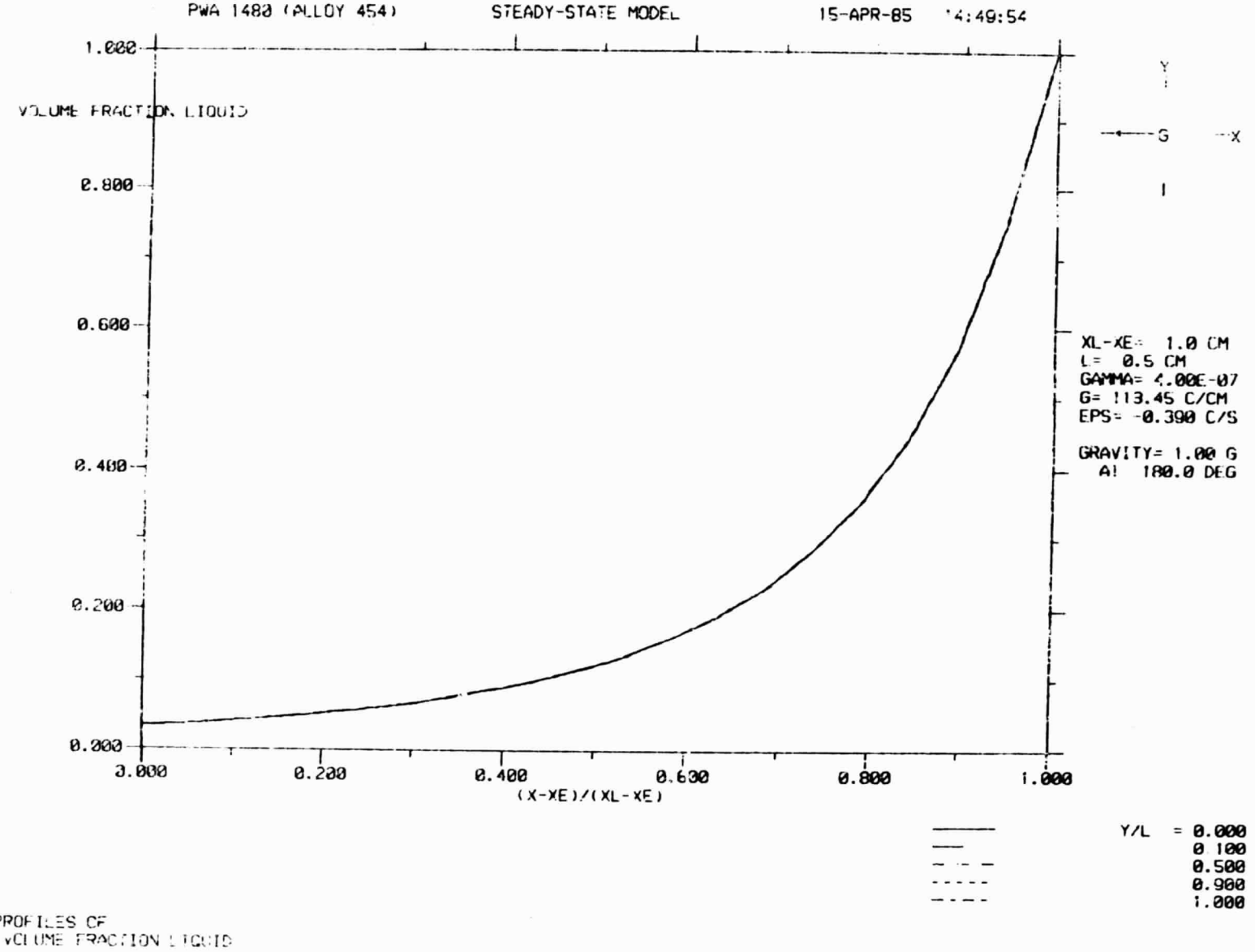

Figure 2.17. Volume Fraction Liquid Across the S/L Zone

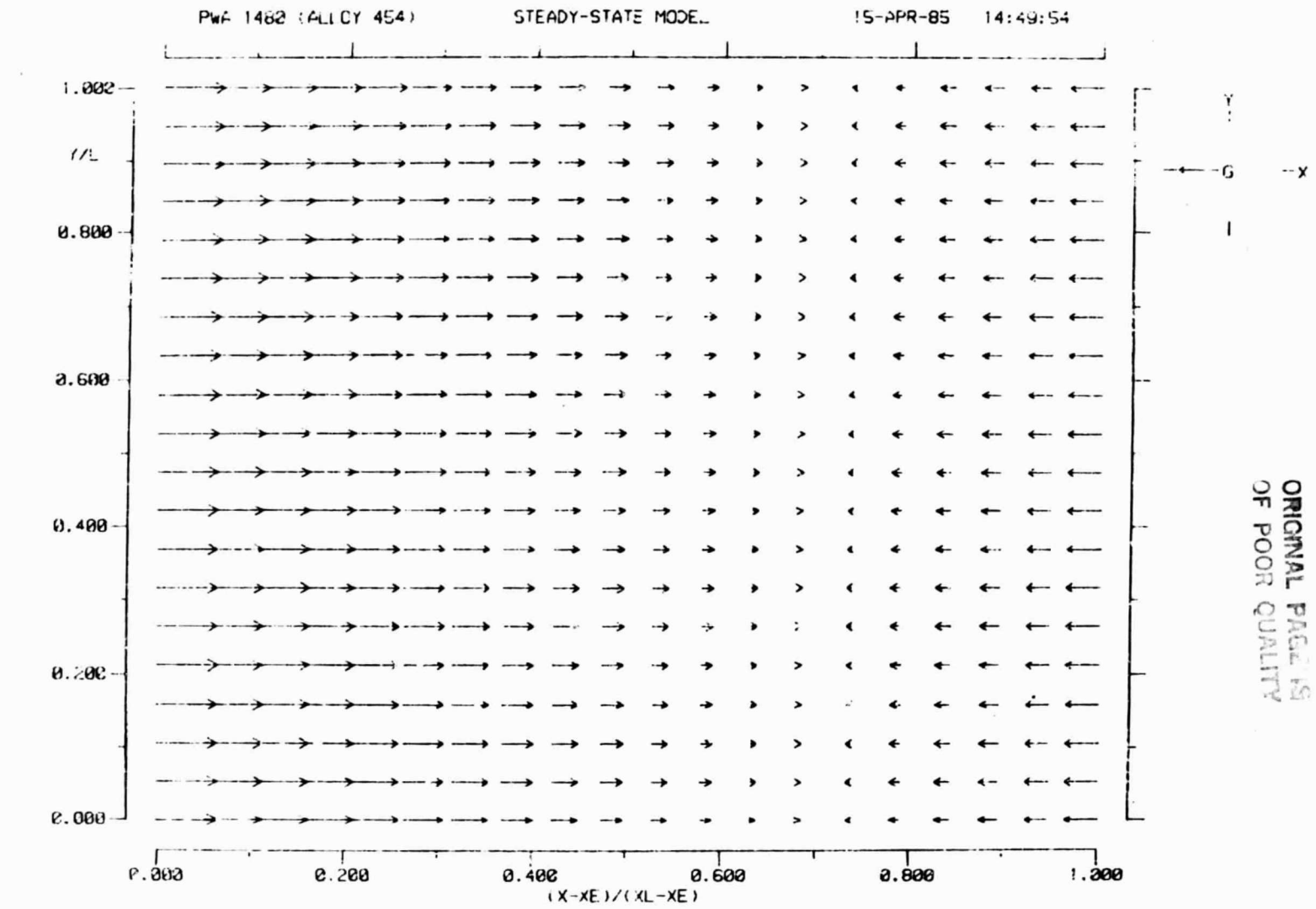

Figure 2.18. Interdendritic Fluid Flow

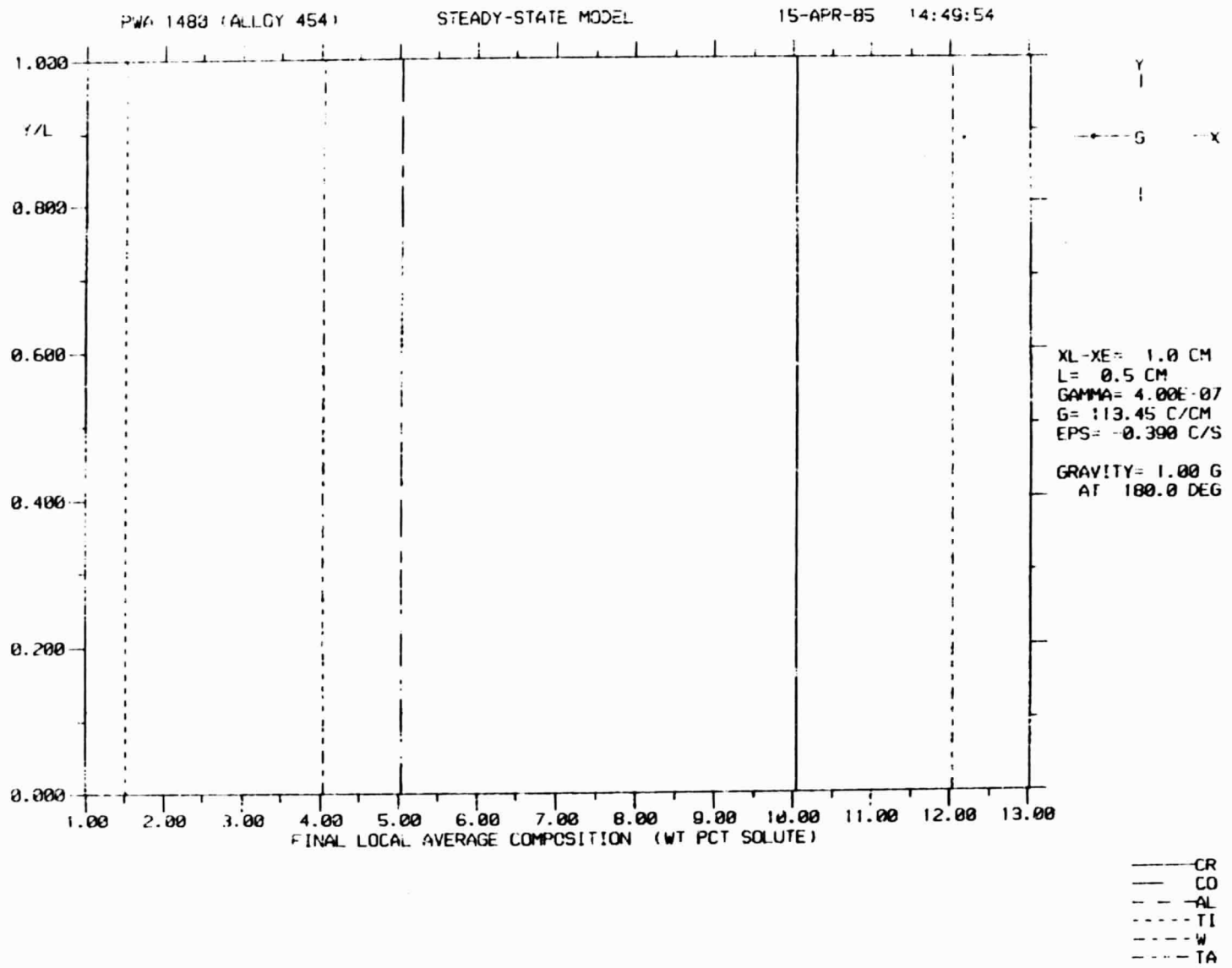

Figure 2.19. Final Local Average Weight Percent of Each Element

2.2.2 UNSTEADY-STATE EXAMPLE

The output shown here is the same plot selection as for MAR-M246 shown in Ref. 3 and for MAR-M246(Hf) shown in Section 2.12. The first two plots (Fig. 2.20 and 2.21) show the interdendritic fluid flow in the S/L zone and contours of the weight percent of chromium in the final solid when the solidus has progressed to 3 cm from the chill and the liquidus is at 4 cm from the chill. The remaining plots (Fig. 2.22 through 2.27) show the vertical profile of each element in the solidified casting. Because the solidification is vertical, there is essentially no segregation except for the inverse segregation near the chill.

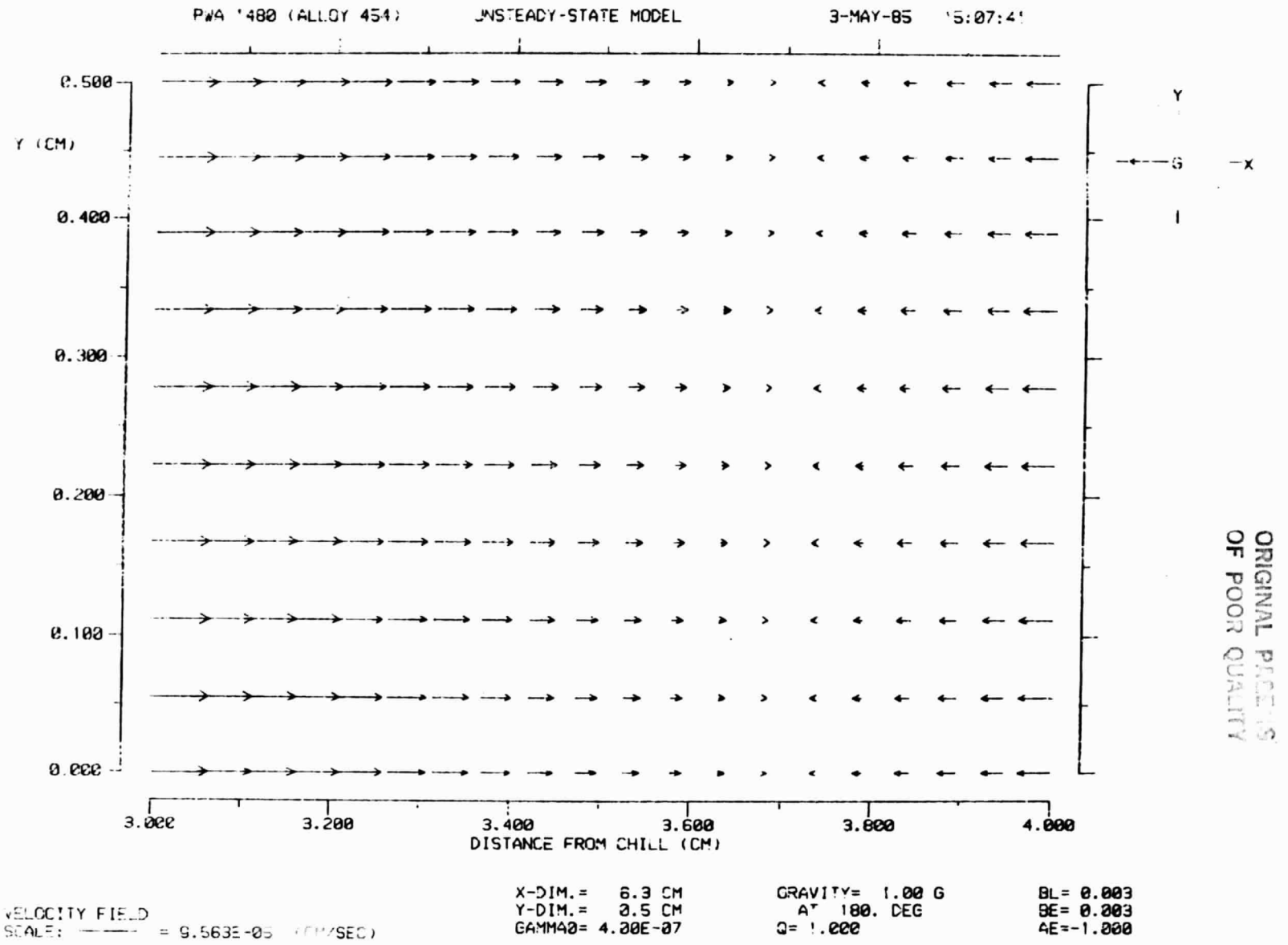

Figure 2.20. Interdendritic Fluid Flow in S/L Zone (Plot 1)

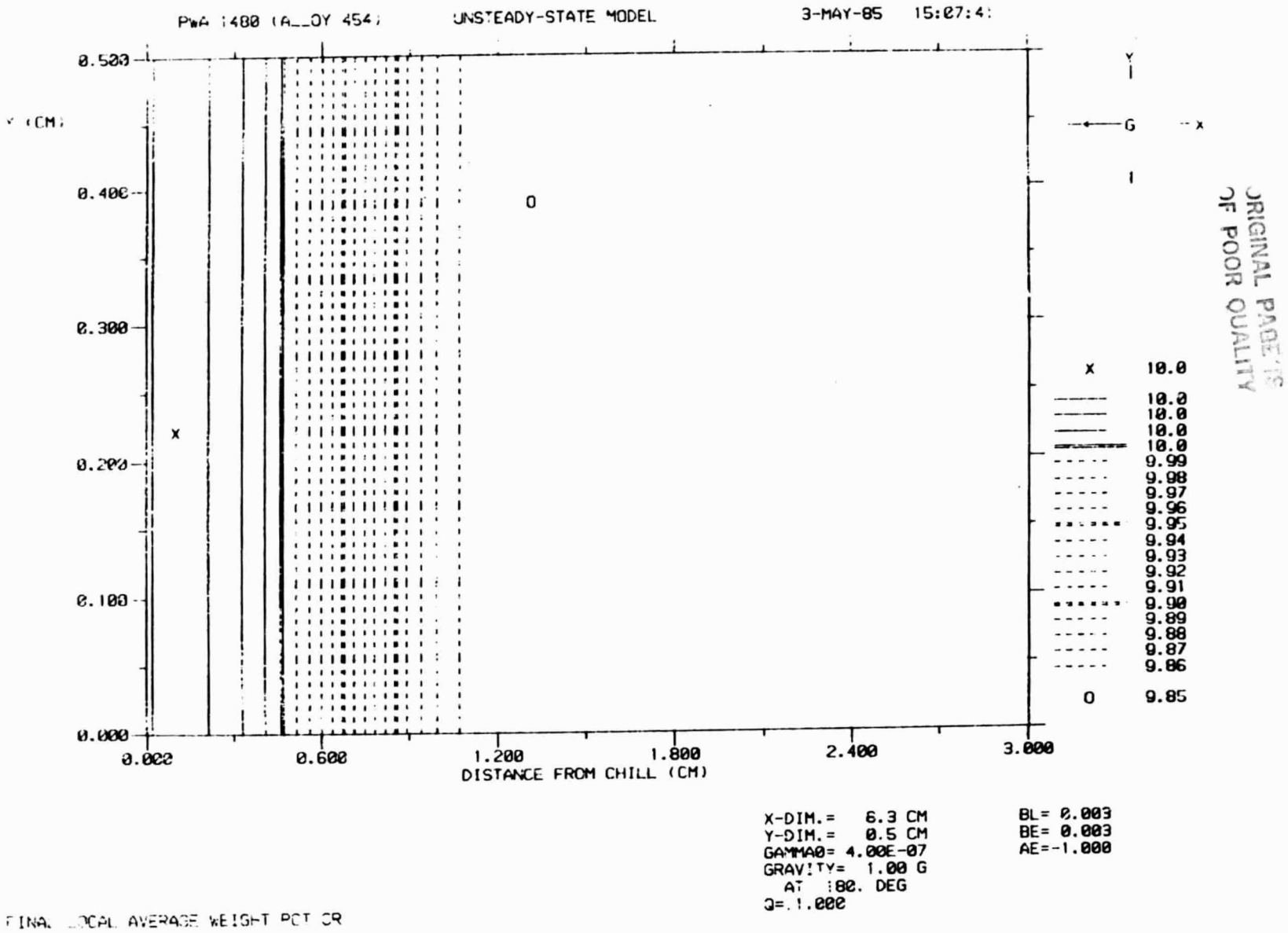

Figure 2.21. Contours of the Weight Percent of Chromium (Plot 2)

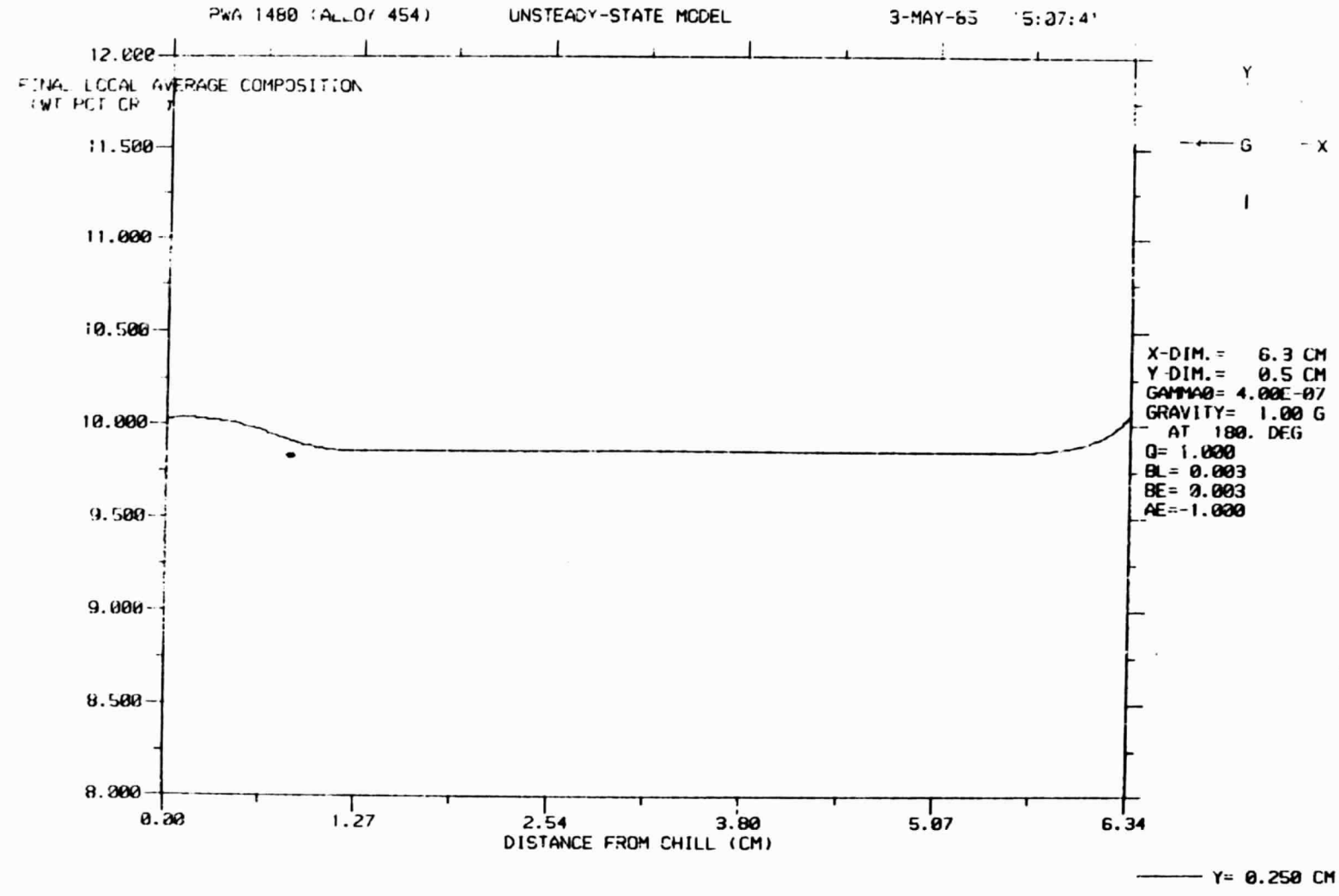

Figure 2.22. Vertical Profile of Each Element in Solidified Casting (Plot 3)

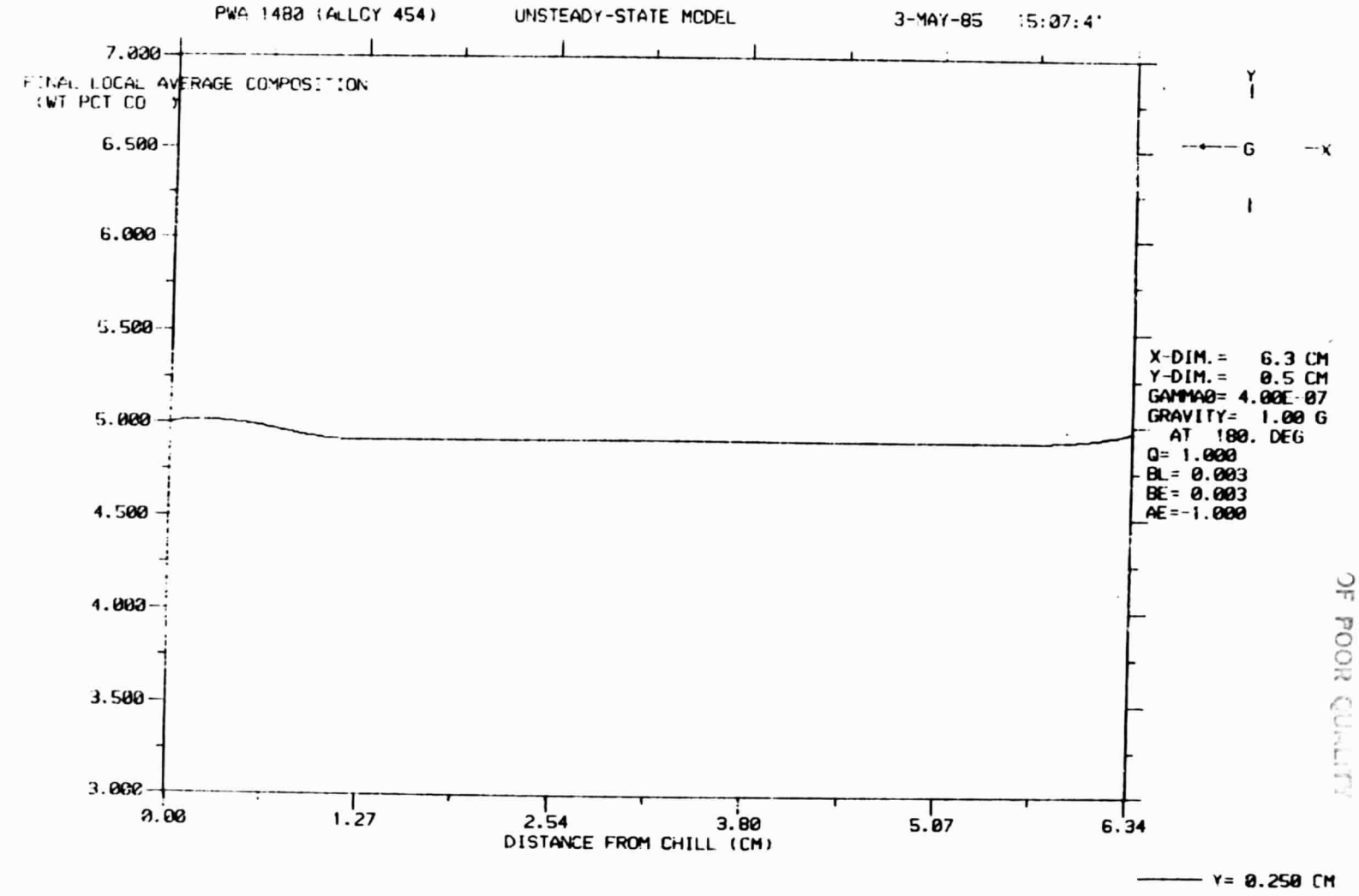

Figure 2.23. Vertical Profile of Each Element in Solidified Casting (Plot 4)

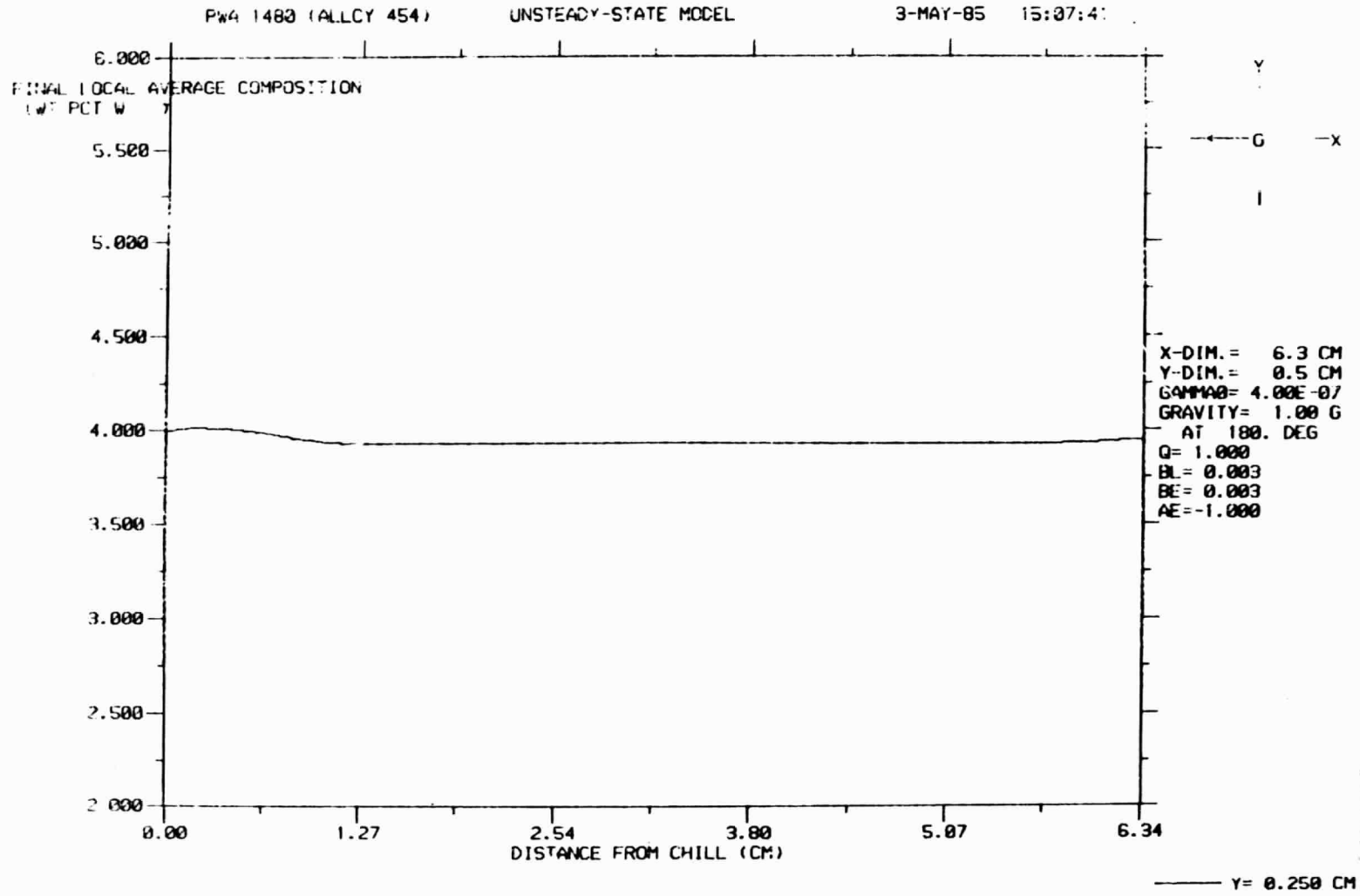

Figure 2.24. Vertical Profile of Each Element in Solidified Casting (Plot 5)

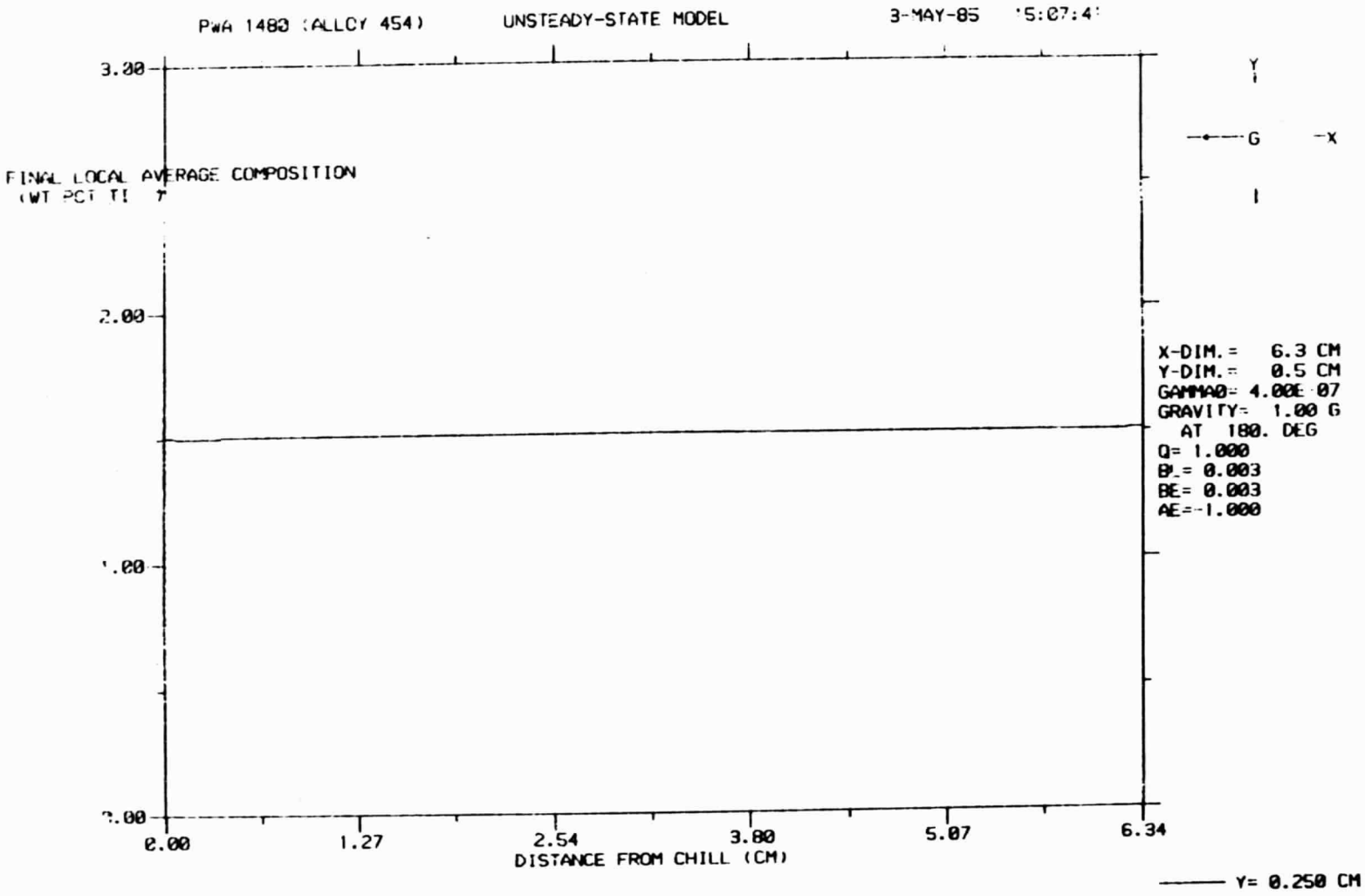

XE = 6.33832 XL = 7.33832
TIME = 2446. SEC

Figure 2.25. Vertical Profile of Each Element in Solidified Casting (Plot 6)

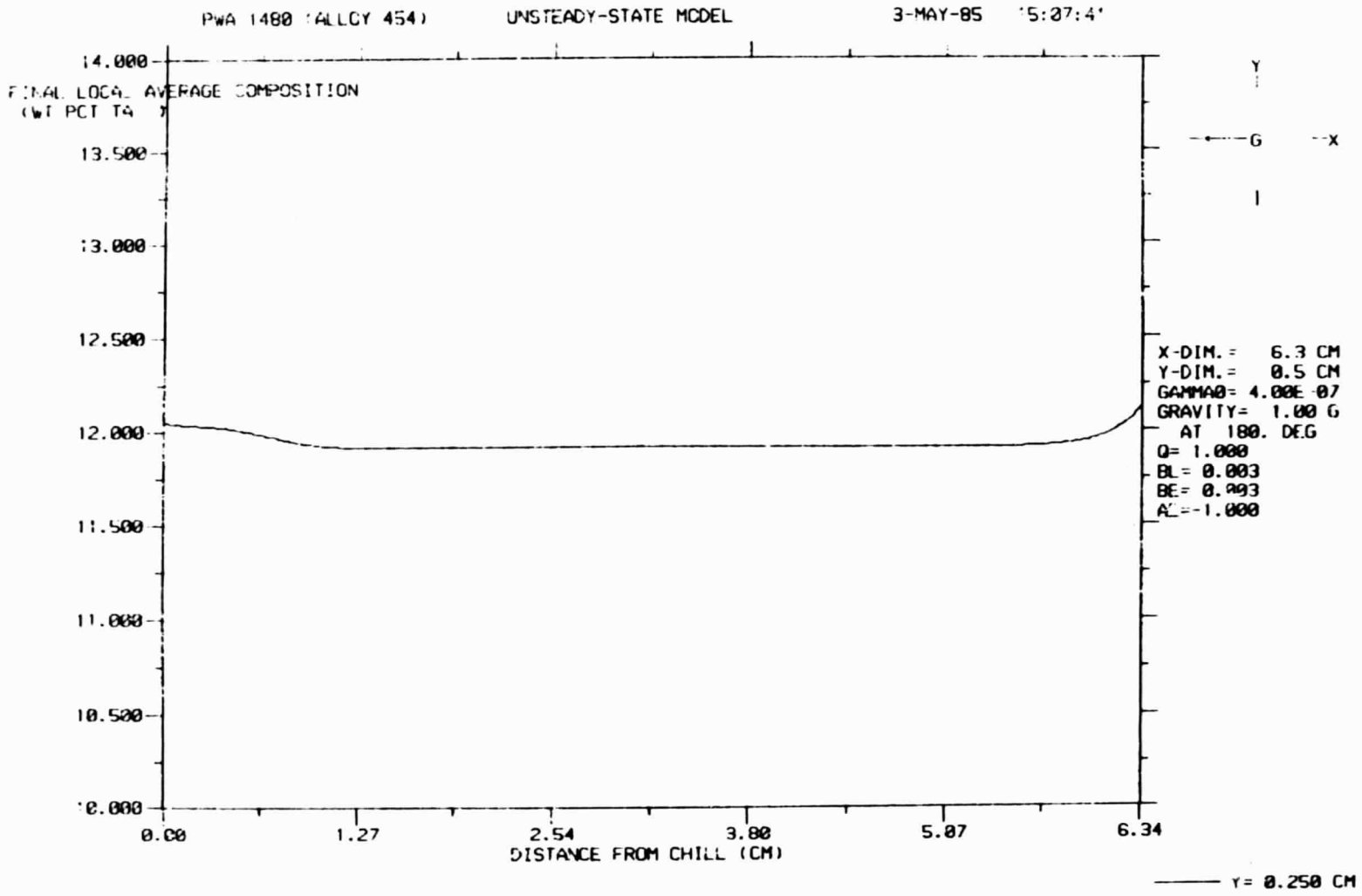

Figure 2.26. Vertical Profile of Each Element in Solidified Casting (Plot 7)

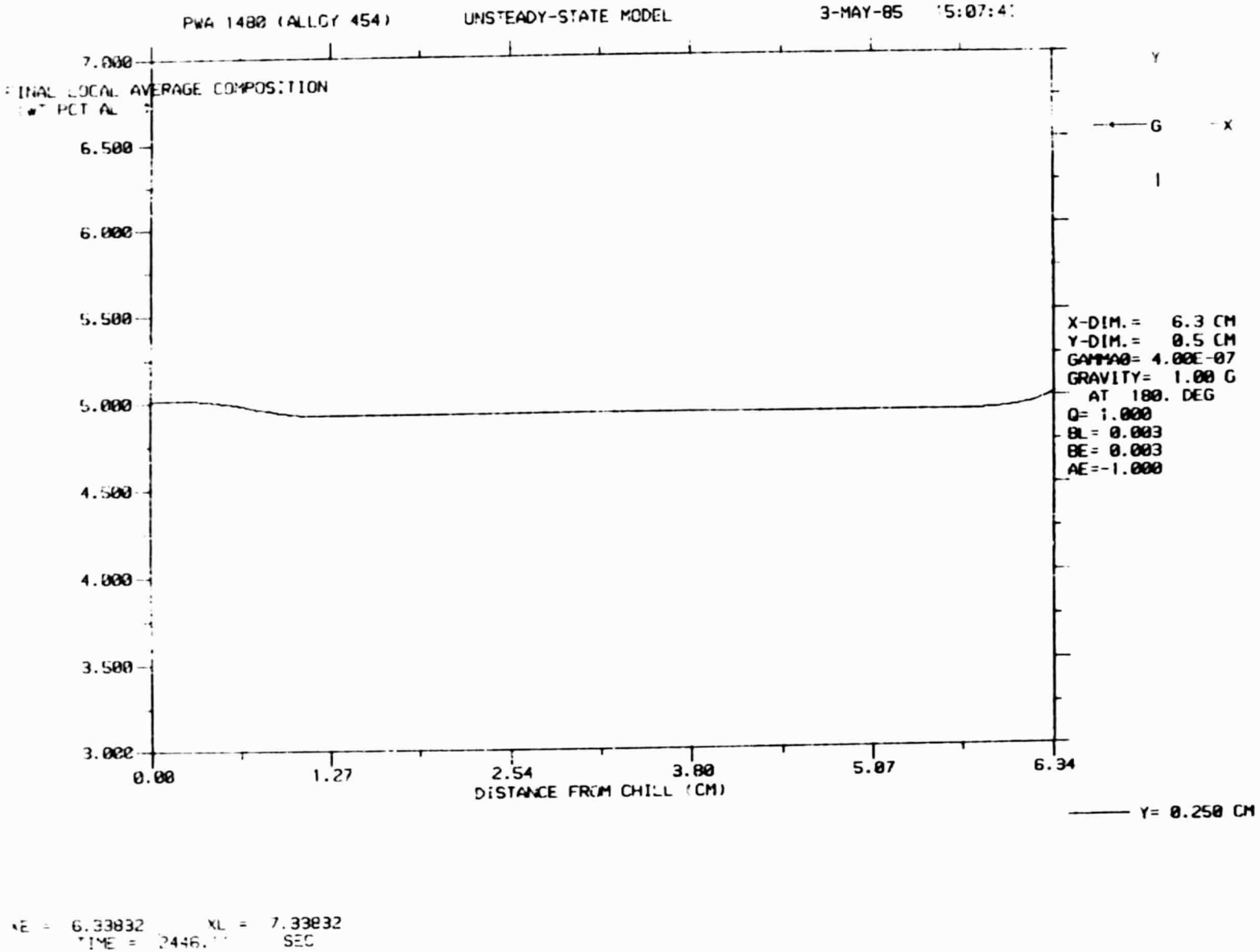

Figure 2.27. Vertical Profile of Each Element in Solidified Casting (Plot 8)

SECTION 3
POROSITY PREDICTION

A new selection was added to the graphical output of all four models. The new plot shows the region in the S/L zone where hydrogen bubbles may nucleate. In the steady-state models, this plot may be generated at the end of each case (Fig. 3.1). The plot can be repeated for any input values of ambient pressure and initial amount of dissolved gas, because these values do not affect the solidification calculation. In the unsteady-state models, the porosity plot may be generated at any checkpoint during the solidification while the S/L zone exists (Fig. 3.2).

The model predicts pore formation at a point in the S/L zone if

$$p_G > p_o + p + 2\sigma/r \qquad (3.1)$$

where

- p_G = partial pressure of dissolved gas,
- p_o = ambient pressure,
- p = pressure due to fluid flow and metallostatic height,
- σ = surface tension, and
- r = bubble radius.

Discussions of the inequality (3.1) and of porosity in Al-Cu alloys can be found in Ref. 4 and 5.

Before each plot is generated, the user is asked to input the ambient pressure and the initial concentration of hydrogen in the liquid metal (Fig. 3.1 and 3.2). The latter is used together with data on the solubility of hydrogen in the alloy to calculate the partial pressure of dissolved hydrogen in the interdendritic liquid at the given temperature and composition. The solubility data and the liquid metal surface tension are stored in the multicomponent-alloy data base for each alloy. In the binary-alloy models, there is no data base change because only aluminum-copper admits significant amounts of dissolved hydrogen. Calculation details of the partial pressure appear in Appendix C.

```
PWA 1480 (ALLOY 454)          STEADY-STATE MODEL              26-APR-85   13:57:20

     FUNCTION TO PLOT                                    PLOT TYPE

  1  FINAL LOCAL AVERAGE COMPOSITION                  1  Y - PROFILES
  2  MACROSEGREGATION                                 2  X - PROFILES
  3  VELOCITY                                         3  VECTOR FIELD
  4  PRESSURE: P-P0
  5  PRESSURE - BULK HYDROSTATIC P
  6  FRACTION LIQUID
  7  MASS FLOW
  8  SOLUTE FLOW
  9  POROSITY


ENTER ITEM NUMBER OF FUNCTION TO PLOT, OR
      P TO PROCEED.



Estimate of regions affected by gas-caused porosity
(Valid for hydrogen only.)

Enter ambient pressure (atmospheres): 1.

Enter amount of dissolved gas initially present in molten metal (wt. pct.): 5.E-4
```

Figure 3.1. Selection of Porosity-Prediction Graphics in Steady-State Models

```
PWA 1480 (ALLOY 454)        UNSTEADY-STATE MODEL              15-MAY-85   15:34:45

     FUNCTION TO PLOT                                    PLOT TYPE

**********       S/L ZONE       **********           1  Y PROFILES
  1  VELOCITY                                         2  X PROFILES
  2  PRESSURE: P-P0                                   3  VECTOR FIELD
  3  PRESSURE - BULK HYDROSTATIC P                    4  CONTOURS
  4  FRACTION LIQUID
  5  MASS FLOW
  6  SOLUTE FLOW
  7  POROSITY

**********          INGOT       **********
  8  FINAL LOCAL AVERAGE COMPOSITION
  9  VOLUME FRACTION EUTECTIC


ENTER ITEM NUMBER OF FUNCTION TO PLOT, OR
      P TO PROCEED.


Estimate of regions affected by gas-caused porosity
(Valid for hydrogen only.)

Enter ambient pressure (atmospheres): 1.

Enter amount of dissolved gas initially present in molten metal (wt. pct.): 2.E-6
```

Figure 3.2. Selection of Porosity-Prediction Graphics in Unsteady-State Models

3.1 BINARY ALLOYS

The only binary alloy system for which the models make porosity prediction is aluminum-copper. Appendix E shows the development of the equations for the partial pressure of hydrogen dissolved in the interdendritic liquid of solidifying aluminum-copper alloys. Appendix F presents the calculation of the surface tension of the interdendritic liquid. The constant coefficients from these two calculations were not put into the binary-alloy data base because the form of the equations probably would not generalize to other binary alloy systems which exhibit gas-caused porosity. Aluminum-copper is the only alloy system currently in the binary-alloy data base which admits significant amounts of dissolved hydrogen is aluminum-copper.

Figures 3.3 through 3.5 show the predicted regions of hydrogen bubble nucleation in Al-4.5 wt.pct. Cu undergoing horizontal steady-state solidification. They also illustrate the effect of the ambient pressure and the initial concentration of dissolved gas on the extent of the predicted region. In Fig. 3.3, gas bubble nucleation is predicted over about 40 percent of the S/L zone when the ambient pressure is 1 atm and the initial concentration of hydrogen is 2×10^{-6} wt. pct. In Fig. 3.4, all conditions are the same except that the ambient pressure has been reduced to 10^{-6} atm. The model now predicts bubble nucleation over about 90 percent of the S/L zone. A similar effect is seen in Fig. 3.5 where the ambient pressure is 1 atm, but the initial concentration of hydrogen has been increased to 2×10^{-5} wt. pct.

3.2 MULTICOMPONENT ALLOYS

The form of the partial pressure calculation is the same for all multicomponent alloys currently in the data base. The surface tension and hydrogen interaction data have been added to the data base for each alloy. Porosity predictions for a case of unsteady-state solidification of PWA 1480 follow.

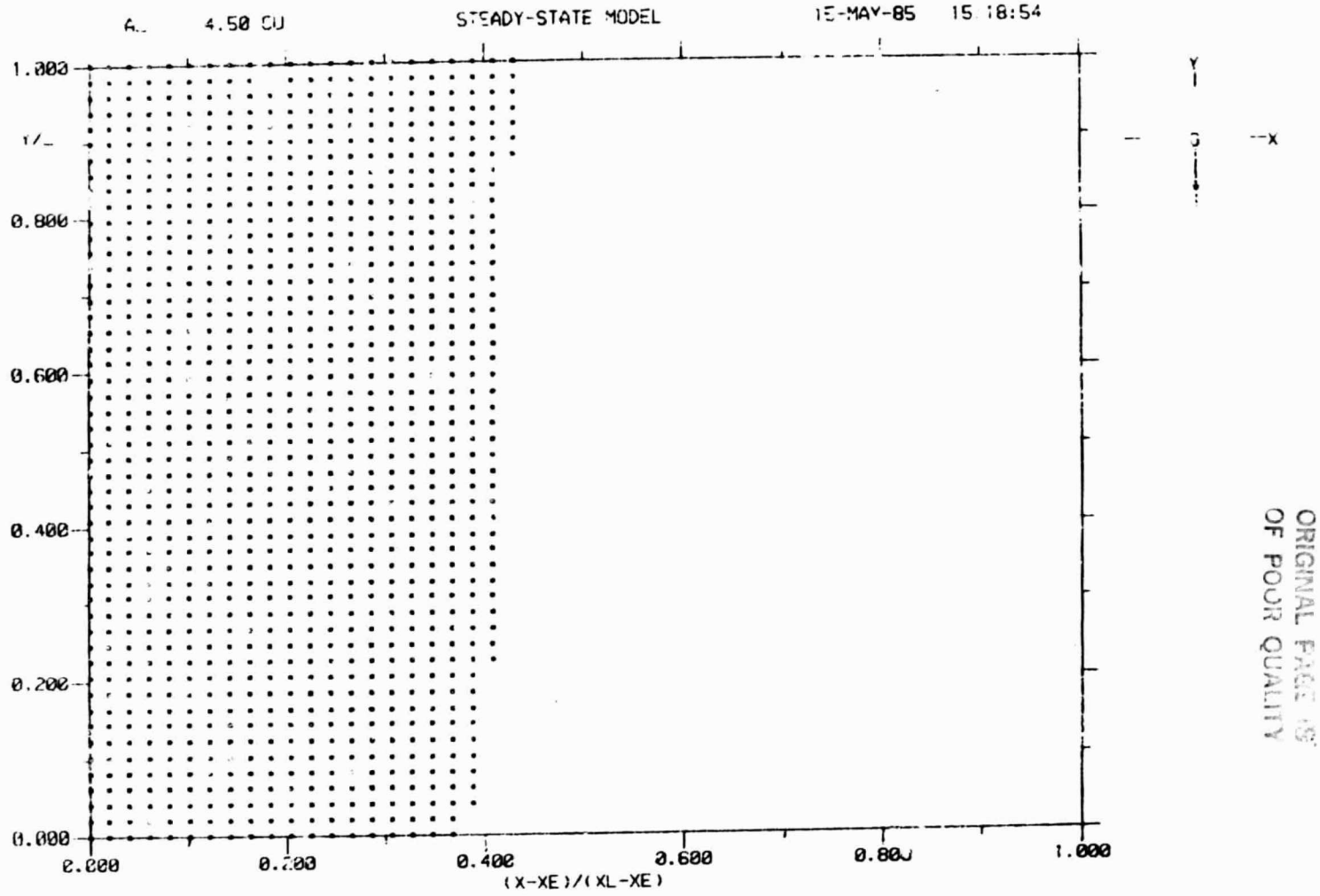

Figure 3.3. Porosity Predictions for Al-4.5 wt.pct. Cu Undergoing Steady-State Horizontal Solidification

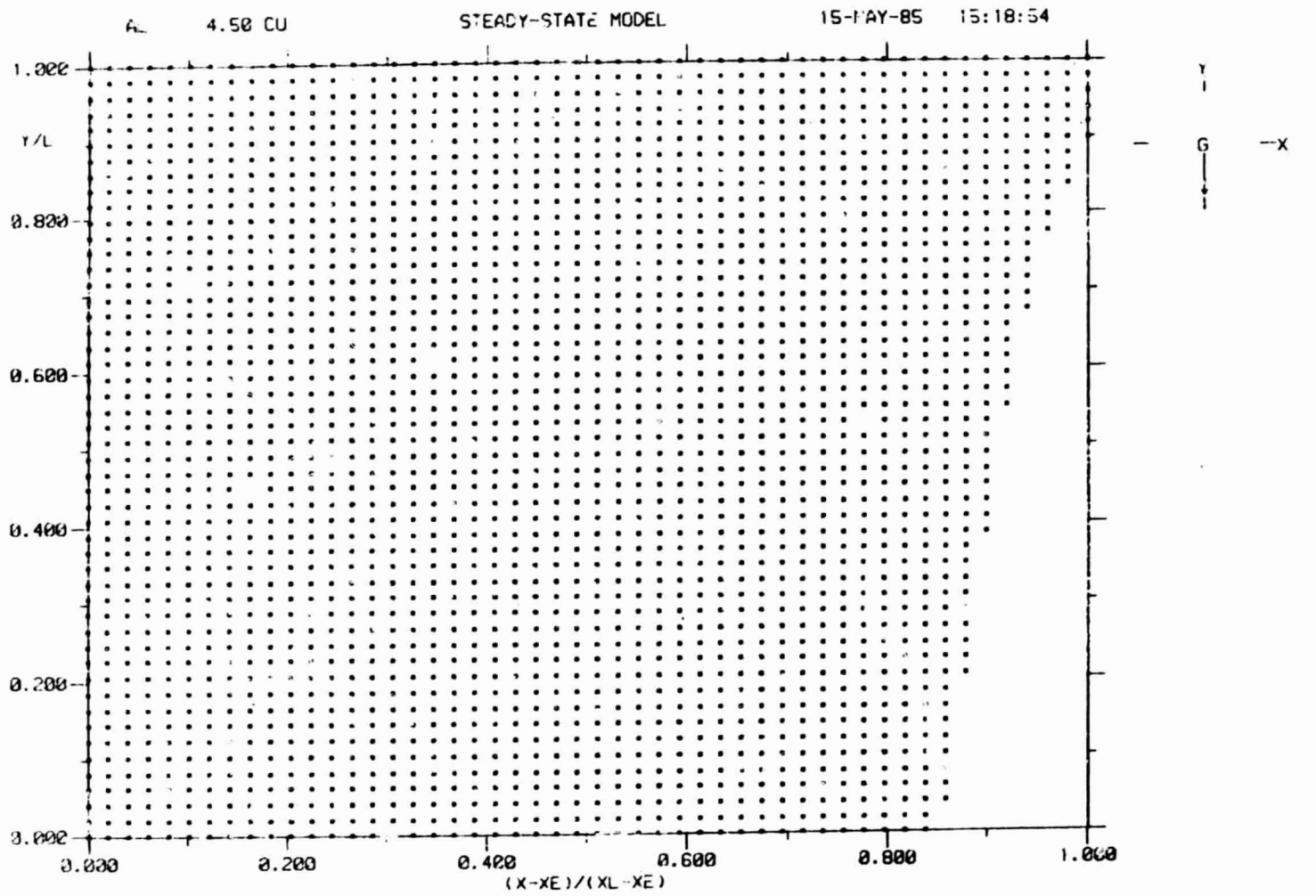

Figure 3.4. Porosity Predictions for Al-4.5 wt.pct. Cu Undergoing Steady-State Horizontal Solidification

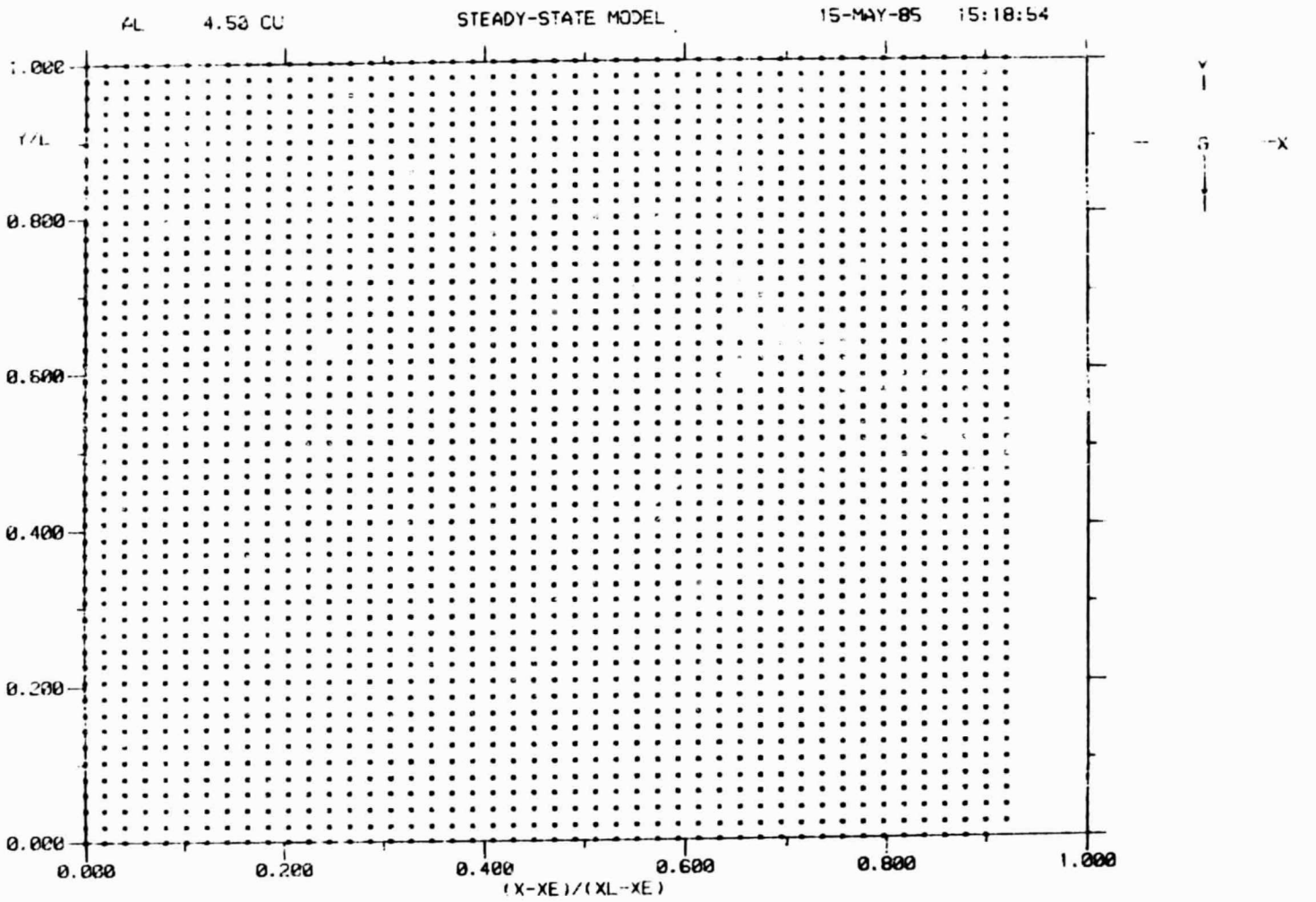

Figure 3.5. Porosity Predictions for Al-4.5 wt.pct. Cu Undergoing Steady-State Horizontal Solidification

3.2.1 MODIFICATION TO DATA BASE

The surface tension, σ , and the hydrogen interaction coefficient for each element, e_H^m have been added to the data base. The structure of the multicomponent alloy data base is now:

CARD	FORMAT	CONTENTS
1	A1, 5A4, 14A4	*Alloy name, comment (1st character must be *, alloy name may be up to 20 characters, 56-character component will appear on screen during alloy selection)
2	15, 5X, 7E10.4	N_m, T_{mp}, T_E, ρ_s, ρ_{mp}, ρ_{SE}, $\partial\rho_L/\partial T$, σ
3	A4, 6X, 4E10.4	Constituent name, C_{om}, k_m, $\partial T/\partial C_{Lm}$, $\partial\rho_L/\partial C_{Lm}$, e_H^m

Card 3 is repeated for each constituent in the alloy. Cards 1 through 3 are repeated for each alloy.

3.2.2 PWA 1480 EXAMPLE

Figures 3.6 through 3.10 show predictions of regions of hydrogen bubble nucleation in the time-varying S/L zone of PWA 1480 undergoing vertical directional unsteady-state solidification subject to the same input conditions as in the example in Section 2.2.2. In Fig. 3.6, the S/L zone has just begun to form at the chill surface, the liquidus isotherm has only progressed to 0.02 cm from the chill, and the fraction solid at the chill is still small. For an ambient pressure of 1 atm and an initial hydrogen concentration of 8×10^{-4} wt. pct., the model predicts no bubble nucleation in the S/L zone at this point in the solidification. Later, after the liquidus isotherm has progressed to 0.4 cm from the chill, but with some liquid still remaining next to the chill, the model predicts bubble nucleation over about 40 percent of the S/L region (Fig. 3.7). Figures 3.8 through 3.10 show the porosity predictions when the liquidus isotherm is at 0.8, 2.0, and 4.0 cm from the chill. There is no variation in the Y direction, because for directional solidification solidification, the velocity vectors are all vertical; hence, the pressure field is uniform in the Y direction.

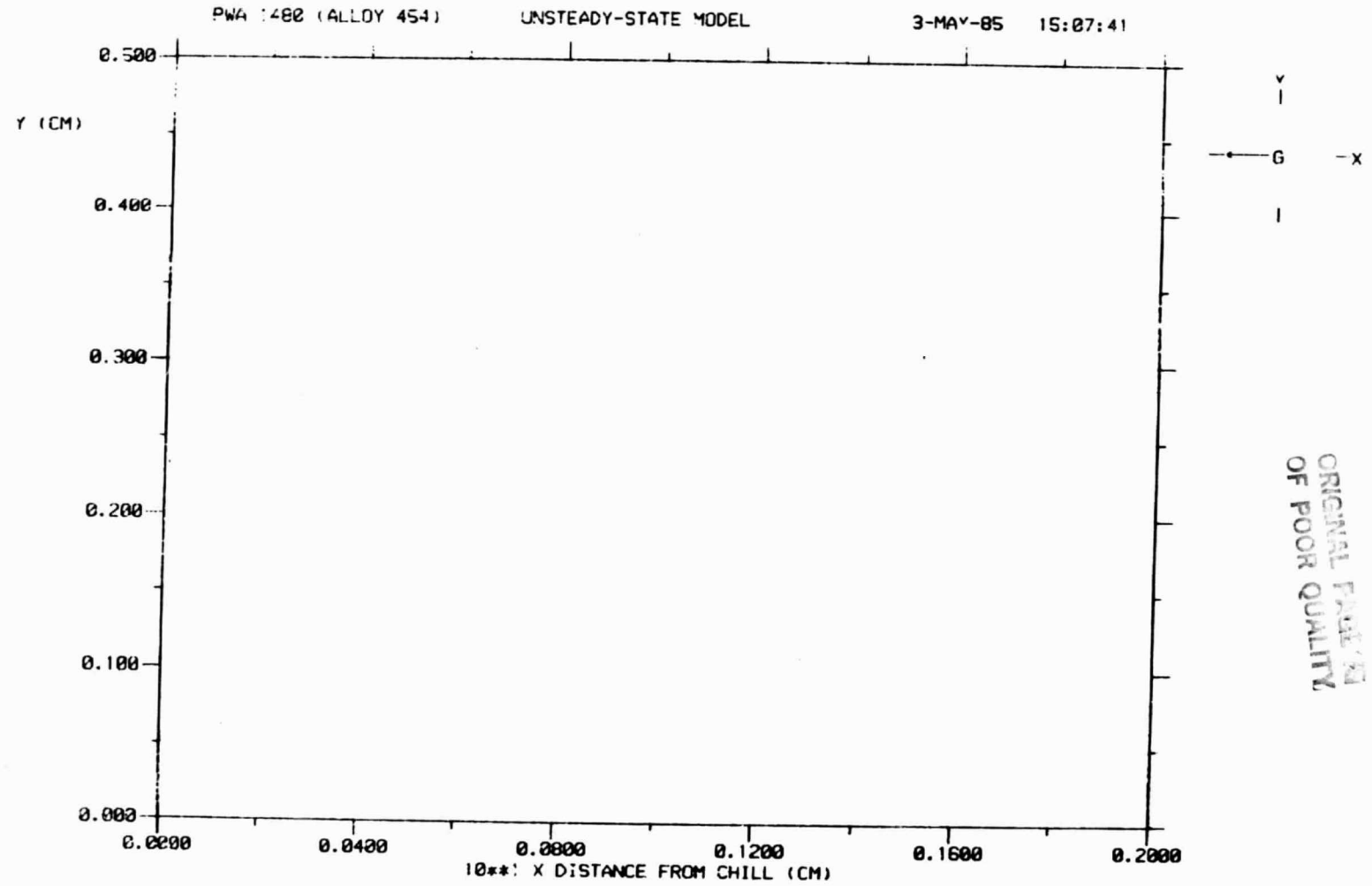

Figure 3.6. Porosity Predictions for PWA 1480 Undergoing Unsteady-State Directional Solidification

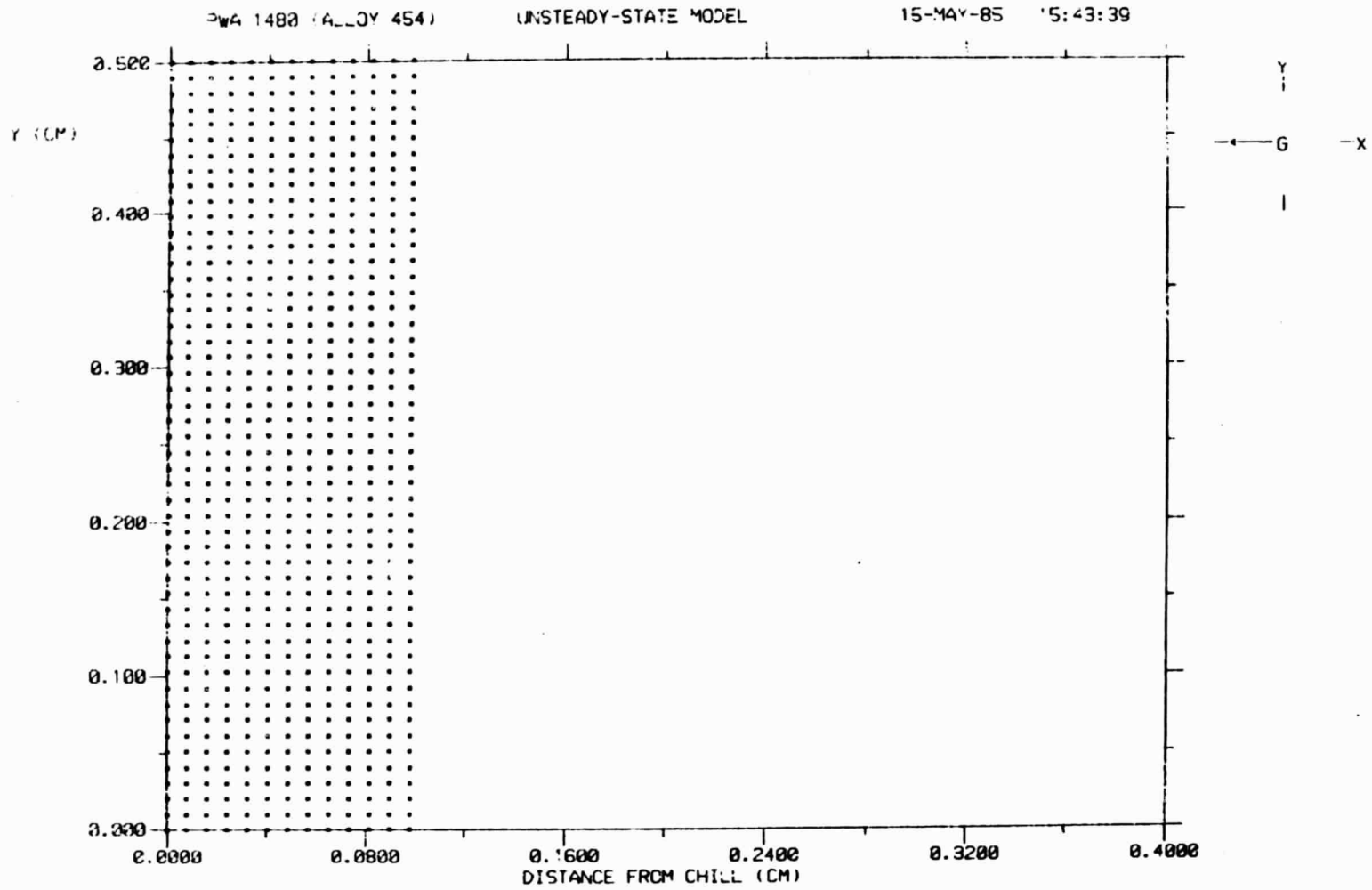

Figure 3.7. Porosity Predictions for PWA 1480 Undergoing Unsteady-State Directional Solidification

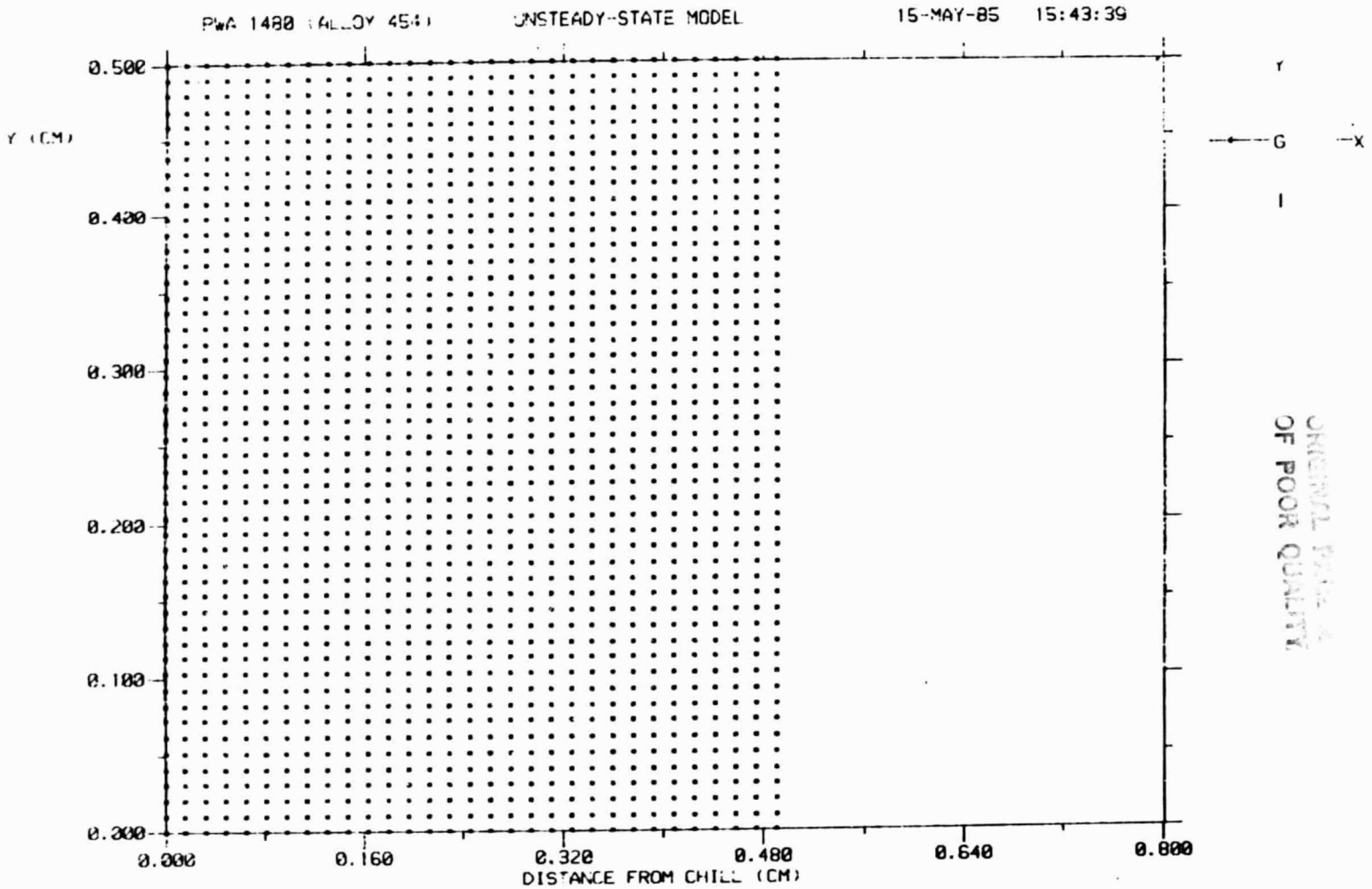

Figure 3.8. Porosity Predictions for PWA 1480 Undergoing Unsteady-State Directional Solidification

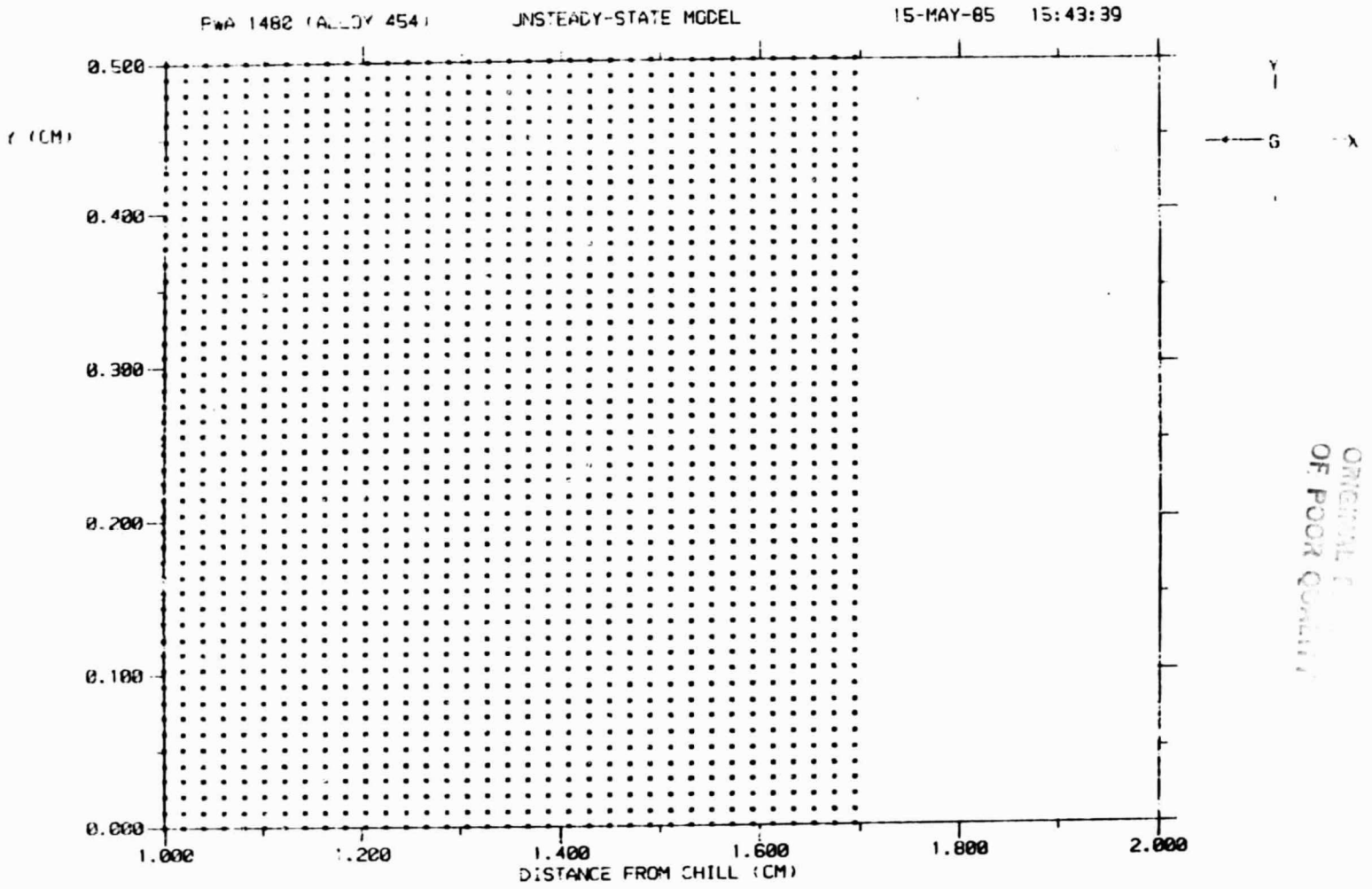

Figure 3.9. Porosity Predictions for PWA 1480 Undergoing Unsteady-State Directional Solidification

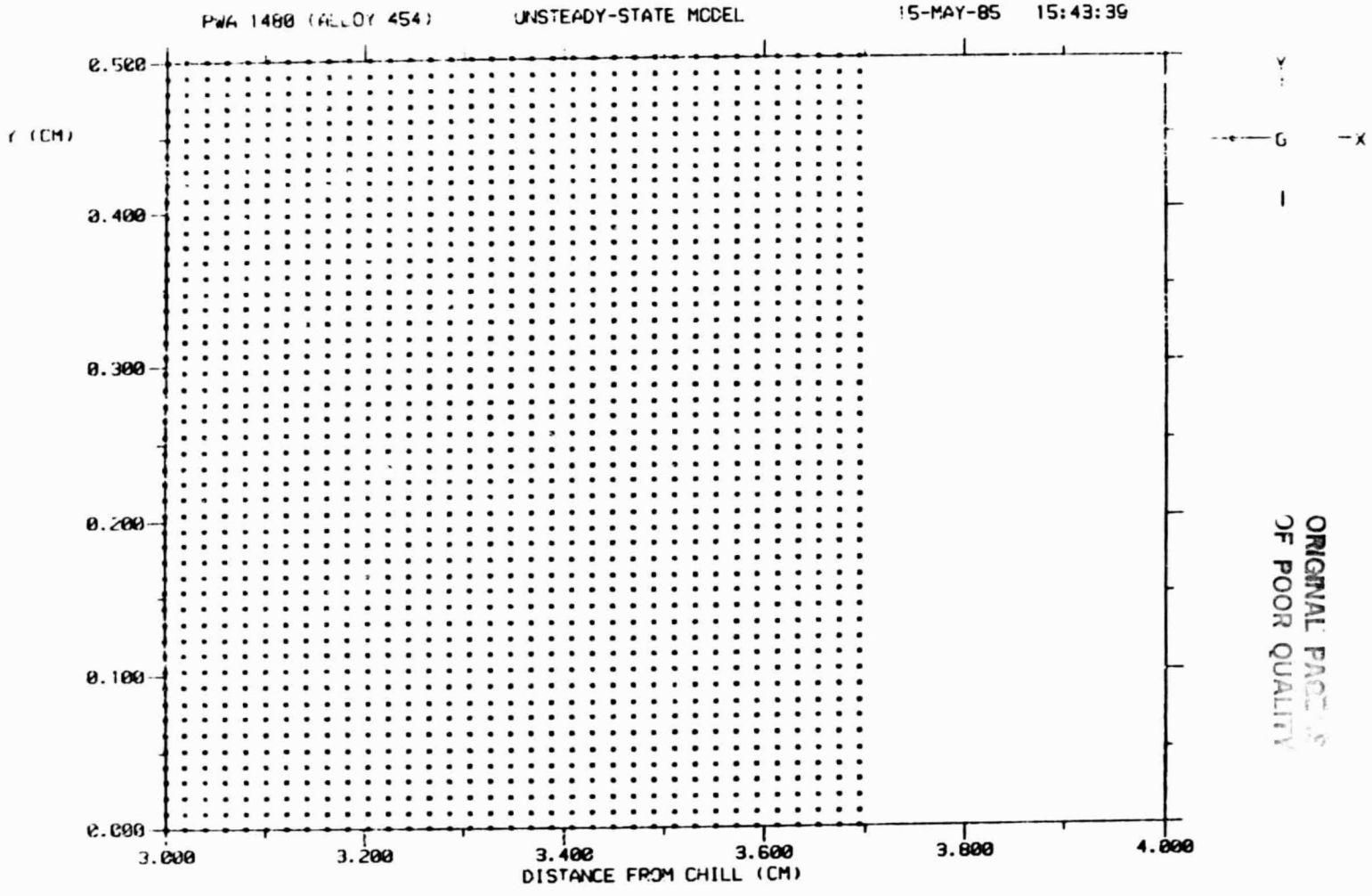

Figure 3.10. Porosity Predictions for PWA 1480 Undergoing Unsteady-State Directional Solidification

SECTION 4
VAX-INSTALLATION OPERATING PROCEDURES AND MAINTENANCE GUIDE

4.1 VAX/VMS SYSTEM USAGE

The materials processing programs have been installed on a Digital Equipment Corporation (DEC) VAX* 11/780 computer at Marshall Space Flight Center. The VAX/VMS operating system is an extremely user-friendly environment; the models can be maintained with little specialized knowledge of the system. This document is intended to help users run the models and make minor modifications of the code. It is recommended that users gain a more comprehensive knowledge of the VAX/VMS system from the available DEC documentation before undertaking extensive program modifications or program development.

4.1.1 SOME COMMANDS

A few rudimentary commands are described in Table 4.1. A good introduction to elementary system use is in the Primer listed in Section 1.2.

Table 4.1. Rudimentary Commands

Command	Description
DELETE filename.typ;n	Deletes version n of file filename.typ.
DIRECTORY	Lists the files in the current default directory. Use the HELP command to learn the DIRECTORY command qualifiers that can provide more information such as file size or creation date.
EDIT filename.typ	Invokes the system text editor. After you are in the editor, you can get help from a HELP command. Use the (EDT) editor in line mode only; screen mode is not compatible with the Tektronix 4014.
HELP	Presents a list of subjects and command names for which information is available. Provides descriptions of commands, command formats, and command qualifiers.
LOGOUT	Logs the current user out of the system.
PURGE filename.typ	Deletes all but the highest version number of file filename.typ.

*VAX is a trademark of Digital Equipment Corporation.

Table 4.1 Rudimentary Commands (Continued)

Command	Description
SET PROT=(O:RWED) filename.typ;n SET PROT=(O:RWE) filename.typ;n	and change the protection codes for a specific file. In the first case delete access is allowed; the second form protects a file from accidental deletion. To determine the current protection of all files enter DIR/PROT.

4.1.2 SOME MANUALS

VAX/VMS Primer
VAX-11 Information Directory and Index
VAX/VMS Command Language User's Guide
EDT Editor Manual
VAX-11 FORTRAN Language Reference Manual
VAX-11 FORTRAN User's Guide

4.2 DESCRIPTION OF FILES

Table 4.2. File Descriptions

File	Description
ALLOYS.DAT	Alloy data base used by models 1 and 2 for binary-systems.
ALLOYS3.DAT	Alloy data base used by model 3.
BELL.FOR BELL.OBJ	Subroutine which rings terminal bell without moving cursor.
FTN.COM	Command file for compiling.
GRAPHICS.OLB	Tektronix software object library.
ICARD.DAT	Input card image read by all programs.
LNK.COM	Command file for linking.
M1.CMN M1.EXE M1.FOR	COMMON blocks for M1. Executable image for M1. FORTRAN source for M1.
M1M.CMN M1M.EXE M1M.FOR	COMMON blocks for M1M. Executable image for M1M. FORTRAN source for M1M.

Table 4.2. File Descriptions (Continued)

File	Description
M2.CMN	COMMON blocks for M2.
M2.EXE	Executable image for M2.
M2.FOR	FORTRAN source for M2.
M2M.CMN	COMMON blocks for M2M.
M2M.EXE	Executable image for M2M.
M2M.FOR	FORTRAN source for M2M.
M3.CMN	COMMON blocks for M3.
M3.EXE	Executable image for M3.
M3.FOR	FORTRAN source for M3.
MALLOYS.DAT	Alloy data base for multicomponent-alloy systems.
MPS.COM	Command file for executing models 1 and 2.
MPS3.COM	Command file for executing model 3.
PLOT10.OLB	Tektronix software object library.
SPARSE.CMN SPARSE.FOR SPARSE.OLB	Sparse matrix routines used by models.

4.3 HOW TO RUN OR MODIFY THE PROGRAMS

To run either the steady-state model or the unsteady-state model, enter the command:

@MPS name where "name" is one of

- 1 binary steady-state model,
- 1M multicomponent steady-state model,
- 2 binary unsteady-state model, or
- 2M multicomponent unsteady-state model.

Specific operating instructions for each model are in the July 1983 '83HV004) report.

To run the coupled-energy model, enter the command:

@MPS3

Specific operating instructions for this model are in the January 1984 (84HV001) report.

Two command files, FTN.COM and LNK.COM, have been written to simplify modification of the programs. This setup is intended only for infrequent, minor program modifications.

1. Use a system text editor to make your changes in M1.FOR, M1M.FOR, M2.FOR, or M2M.FOR. Note that the common blocks for each program are stored in the corresponding .CMN file.

2. Compile the program by using the command
   @FTN program options
   where 'program' is the program name, M1, M1M, M2, or M2M, and 'options' is any valid DCL FORTRAN qualifier such as /OPTIMIZE. 'Options' must begin with a /. You can omit 'options' if you want to use the FORTRAN default values. The original setup was compiled with the default values.

3. Link the program by using the command
   @LNK program options
   where 'program' is the program name as in step 2, and 'options' is any valid DCL LINK qualifier such as /DEBUG. 'Options' must begin with a /. You can omit 'options' if you want to use the LINK default values. The original setup was linked with the default values.

   After linking, it is recommended that you conserve file space by DELEting the file 'program'.OBJ and by PURGing the old version of 'program'.EXE. You may need to change the file protection codes in order to do this. See Section 1.2.

4.4 MAGNETIC TAPES

These instructions tell how to use the VAX/VMS system utility called BACKUP to write or read a tape that contains your entire directory. It is the simplest way to backup your files or to transport them to another VAX, but a tape written by BACKUP cannot be read by any other type of computer.

Before you can write or read a magnetic tape, you must have one mounted on a tape drive. Get in touch with the computer operations people, and provide them with a tape. The term "MAG_TAPE" in the commands below is a logical

equivalence name for the tape drive. The computer operations people can tell you the actual name to use.

4.4.1 HOW TO WRITE A BACKUP TAPE FOR BACKUP OR TRANSPORT

```
ALLOCATE MAG_TAPE
MOUNT/FOREIGN MAG_TAPE
BACKUP [JOHNSTON] MAG_TAPE:SEND.BCK/VERIFY/DENSITY=1600/REWIND
DISMOUNT MAG_TAPE
DEALLOCATE MAG_TAPE
```

4.4.2 HOW TO READ A BACKUP TAPE

```
ALLOCATE MAG_TAPE
MOUNT/FOREIGN MAG_TAPE
BACKUP MAG_TAPE [ ]
DISMOUNT MAG_TAPE
DEALLOCATE MAG_TAPE
```

SECTION 5

REFERENCES

1. A. L. Maples and D. R. Poirier, Report No. 80HV007, Vol. I-III, General Electric Company, Huntsville, AL, 1980.

2. A. L. Maples and D. R. Poirier, Report No. 81HV001, Vol. I-III, General Electric Company, Huntsville, AL, 1981.

3. A. L. Maples and D. R. Poirier, Report No. 83HV004, General Electric Company, Huntsville, Al, 1983.

4. M. C. Flemings, Solidification Processing, McGraw-Hill Book Co., New York, NY, 1974.

5. T. S. Piwonka and M. C. Flemings, Trans. Met. Co. AIME, 1966, Vol. 236, pp. 1157-1165.

6. R. Sellamuthu, Ph.D. Thesis, University of Pittsburgh, Pittsburgh, PA, 1979.

7. W. C. S. Wang, M.S. Thesis, The University of Arizona, Tucson, AZ, 1983.

8. H. D. Brody and D. Apelian (eds.), Modeling of Casting and Welding Processes, The Met. Soc. of AIME, Warrendale, PA, 1981, pp. 313-332.

9. J. F. Elliott, M. Gleisner, and V. Ramakrishna, Thermochemistry for Steelmaking, Vol. II, Addison-Wesley, Reading, MA, 1963, pp. 339-459.

10. Metals Handbook, 9th ed., Vol. 3, American Society for Metals, Metals Park, OH, 1980, pp. 249-250.

11. W. T. Loomis, Ph.D. Dissertation, The University of Michigan, Ann Arbor, MI, 1969.

12. A. J. C. Wilson (ed.), Structure Reports, Vol. 14, N.V.A. Oosthoek's Uitgevers MIJ, Utrecht, 1959, pp. 11, 12.

13. I. I. Kornilov and A. Y. Snetkov, Izvestia Akedmii Naut, 1969, pp. 106-111.

14. R. Kadalbal, J. J. Montoyz-Cruz, and T. Z. Kattamis, Met. Trans. A, 1980, Vol 11A, pp. 1547-1553.

15. M. Gell, D. N. Duhl, and A. F. Giamei, Superalloys Source Book, (M. J. Donachie, ed.), American Society for Metals, Metals Park, OH, 1984, 297-306.

16. G. K. Sigworth, J. F. Elliott, G. Vaughn, and G. H. Geiger, Met. Soc. of the Canadian Institute of Metals, Annual Volume, 1977, pp. 104-110.

17. M. Weinstein and J. F. Elliott, Trans. Met. Soc. AIME, 1963, Vol. 227, pp. 382-393.

18. E. A. Brandes (ed.), Smithells Metals Reference Book, 6th ed., Butterworths, London, 1983, pp. 12-2 to 12-6.

19. E. A. Brandes (ed.), ibid., pp. 14-7, 8.

20. E. A. Guggenheim, Trans, Faraday Soc., 1945, vol. 41, p. 150.

21. R. Speiser and J. W. Spretnak, Stress Corrosion Cracking & Embrittlement (W. D. Robertson, ed.), John Wiley & Sons, New York, 1956 pp. 92-106.

22. R. Speiser, The University of Arizona, private communication.

23. E. A. Brandes (ed.), ibid., pp. 14-7, 8.

24. E. T. Turkdogan, Physical Chemistry of High Temperature Technology, Academic Press, New York, 1980, p. 98.

APPENDIX A

DATA FOR MAR-M246(Hf)

A.1 NOMINAL COMPOSITION

Element	wt. pct.	Element	wt. pct.
Cr	9.0	Mo	2.5
Co	10.0	Ta	1.5
Al	5.5	C	0.15
Ti	1.5	Hf	1.5
W	10.0	Ni	bal.

A.2 PARTITION RATIOS

Element	Ratio, k	Source
Cr	0.9	Sellamuthu (6) in MAR-M200; Wang (7) in NASAIR-100
Co	1.1	Jeanfils et al. (8) in Waspalloy
Al	1.1	Sellamuthu (6) in MAR-M200(Hf)
Ti	0.95	Sellamuthu (6) in MAR-M200(Hf)
W	1.2	Sellamuthu (6) in MAR-M200(Hf)
Mo	0.65	Wang (7) in NASAIR-100
Ta	0.97	Elliott et al. (9) in Ni-Ta binary
C	0.25	Jeanfils et al. (8) in Waspalloy
Hf	0.23	Sellamuthu (6) in MAR-M200(Hf)

A.3 TEMPERATURE DURING SOLIDIFICATION

The temperature during solidification is assumed to vary linearly with composition according to

$$T - T_o = \sum_{i=1}^{n} \left(\partial T / \partial C_i \right) \left(C_i - C_{oi} \right) \qquad (A.1)$$

where

n = number of solute elements,

T = temperature (liquidus temperature of the interdendritic liquid), °C,

T_o = liquidus temperature of the reference alloy, °C,

C_i = composition of solute i, wt. pct.,

C_{oi} = composition of solute i in the reference alloy, wt. pct., and

$(\partial T/\partial C_i)$ = change in the liquidus temperature due to solute i, °C/wt. pct.

As in the previous report (3), values of $(\partial T/\partial C_i)$ for most of the solutes were obtained from the binary phase diagrams (Ni - X) in Elliot et al. (9). For hafnium, $(\partial T/\partial C_{Hf})$ was deduced from Sellamuthu's data on MAR-M200 containing 0-2.66 wt. pct. Hf (6).

Element	C_{oi} wt. pct.	$\partial T/\partial C_i$ °C/wt. pct.
Cr	9.0	-2.2
Co	10.0	0.0
Al	5.5	-3.2
Ti	1.5	-7.7
W	10.0	+3.5
Mo	22.5	-1.0
Ta	1.5	-61.0
C	0.15	-2.5
Hf	1.5	-10.4

For MAR-M246, the liquidus temperature (T_o) is 1360°C (10); therefore,

$$\begin{aligned} T = 1360 &-2.2\,(C_{Cr} - 9) - 3.2\,(C_{Al} - 5.5) \\ &-7.7\,(C_{Ti} - 1.5) + 3.5\,(C_{W} - 10) \\ &-2.5\,(C_{Ta} - 1.5) - 1.0\,(C_{Mo} - 2.5) \\ &- 61\,(C_{C} - 0.15) - 10.4\,C_{Hf} \end{aligned} \qquad \text{(A.2)}$$

To apply Eq. (A.2) during solidification, the composition of each element in the interdentritic liquid is computed and Eq. (A.2) is assumed to apply until the temperature drops to 1230°C. At 1230°C, the remaining interdendritic liquid solidifies as eutectic solid.

The temperature of 1230°C was selected after consulting Sellamuthu (6) who reports that MAR-M200 with 1.5 wt. pct. Hf solidifies with 0.10 fraction eutectic (in the absence of macrosegregation). Then by assuming complete diffusion of carbon in the solid and no diffusion of the substitutional elements, a Scheil-type calculation shows that the fraction of interdendritic liquid is 0.10 at a temperature of 1230°C.

A.4 DENSITY OF THE LIQUID

From the previous report (3), the change in density attributed to each of the solutes (excluding Hf) is given. The effect of Hf can be deduced by making use of Table 21 in Sellamutha (6); however, his data for 0.86 wt. pct. Hf appear to be in error and are not used.

For MAR-M200 (without Hf), the density is 7.56 g · cm^{-3} at 1392°C. Using the melt compositions as the reference compositions, given by Sellamuthu (6), we have

$$\begin{aligned}\rho_L = 7.56 &- 0.013\,(C_{Cr} - 8.08) + 0.001\,(C_{Co} - 9.31) \\ &- 0.11\,(C_{Al} - 4.85) - 0.035\,(C_{Ti} - 1.88) \\ &+ 0.033\,C_{Mo} + 0.042\,(C_W - 12.76) \\ &- 0.72\,(C_c - 0.15) + 0.012\,(C_{Nb} - 1.05) \\ &+ 0.035\,C_{Ta} + 0.052\,C_{Hf} \\ &- 0.00125\,(T - 1392) \qquad (A.3)\end{aligned}$$

Here ρ_L is the density of the interdendritic liquid (g · cm^{-3}) and T is the temperature calculated with Eq. (A.2). The coefficients of the composition terms are the respective values of $(\partial\rho/\partial C_i)$ and the coefficient of the temperature term is $(\partial\rho/\partial T)$.

A.5 DENSITY OF THE SOLID

The density of the solid during solidification was computed by using the scheme presented in Appendix A of the previous report (3). In this report, however, some of the coefficients in the equation for the lattice parameter have been changed. As before,

$$a = a_{Ni} + \sum_{i=1}^{n} (da/dX_i)\,X_i \qquad (A.4)$$

where

a_{Ni} = 3.5236 Å

a = lattice parameter (cube-edge length in f.c.c. Ni), and

X_i = atom fraction of solute i.

The coefficients (da/dX_i) are from the following sources:

Element	da/dX_i, Å	Source
Cr	0.105	Loomis (11)
Co	0.019	Loomis (11)
Al	0.186	Loomis (11)
Ti	0.337	Loomis (11)
Mo	0.435	Loomis (11)
W	0.412	Loomis (11)
C	0.065	Structure Reports (12)
Nb	0.645	Loomis (11)
Ta	1.04	Calc. from at. radii
Hf	0.75	Kornilov and Snetkov (13)

The value for hafnium is assumed to be equal to that for zirconium since these two elements are chemically similar and have equal atomic radii.

With the lattice parameter calculated according to Eq. (A.4), the densities of the nickel-rich phase (γ) at 20°C were calculated. Compositions selected were those corresponding to Scheil-type solidification.

The densities of γ at the elevated temperatures in the solidification range were then calculated by using the expansion coefficients presented in the previous report (3).

The density of the eutectic-solid is not available so a calculation using a number of simplifying assumptions was made. The first assumption is that eutectic-solidification occurs isothermally at 1230°C. From the work of Sellamuthu (6), the eutectic comprises $\gamma + \gamma'$ and carbides in MAR-M200 with 2 wt. pct. Hf. To estimate the portion of the eutectic which is carbide, we assume that the carbon remaining in the interdendritic liquid reacts completely to form HfC at 1230°C. According to this simple calculation, the eutectic comprises approximately 2.5 pct. HfC and the balance is a mixture of γ/γ'. Using the composition of the γ/γ', the calculated density is 8.052 g/cm^3 at 1230°C. The small amount of carbide in the eutectic is ignored; therefore, the density of the eutectic solid is 8.052 $g \cdot cm^{-3}$.

A.6 SUMMARY OF DENSITIES

Figure A.1 summarizes the calculated densities of the liquid- and solid-phases during solidification. Figure A.1 gives the densities versus temperature; it shows that the behavior of MAR-M246 (Hf) is substantially different than MAR-M246 without Hf. With 1.5 wt. pct. Hf, the total density change of the interdendritic liquid increases by only 4.5 pct., whereas with no Hf the density of the interdendritic liquid decreases by 16 pct. (see Fig. A.2 in the previous report (3)). With hafnium, the density of the solid is approximately the same as that for the alloy without hafnium.

The effect of hafnium on the density is attributed to its direct effect on increasing density and, also, to its effect on the partition ratios of some of the other elements (especially Al and Ti).

For the calculation of convection and macrosegregation, it is recommended that Eqs. (A.2) and (A.3) be used to calculate the density of the liquid (ρ_L). The recommended values for the solid-densities are $\rho_s = 7.82\ g \cdot cm^{-3}$ and $\rho_{SE} = 8.05\ g \cdot cm^{-3}$.

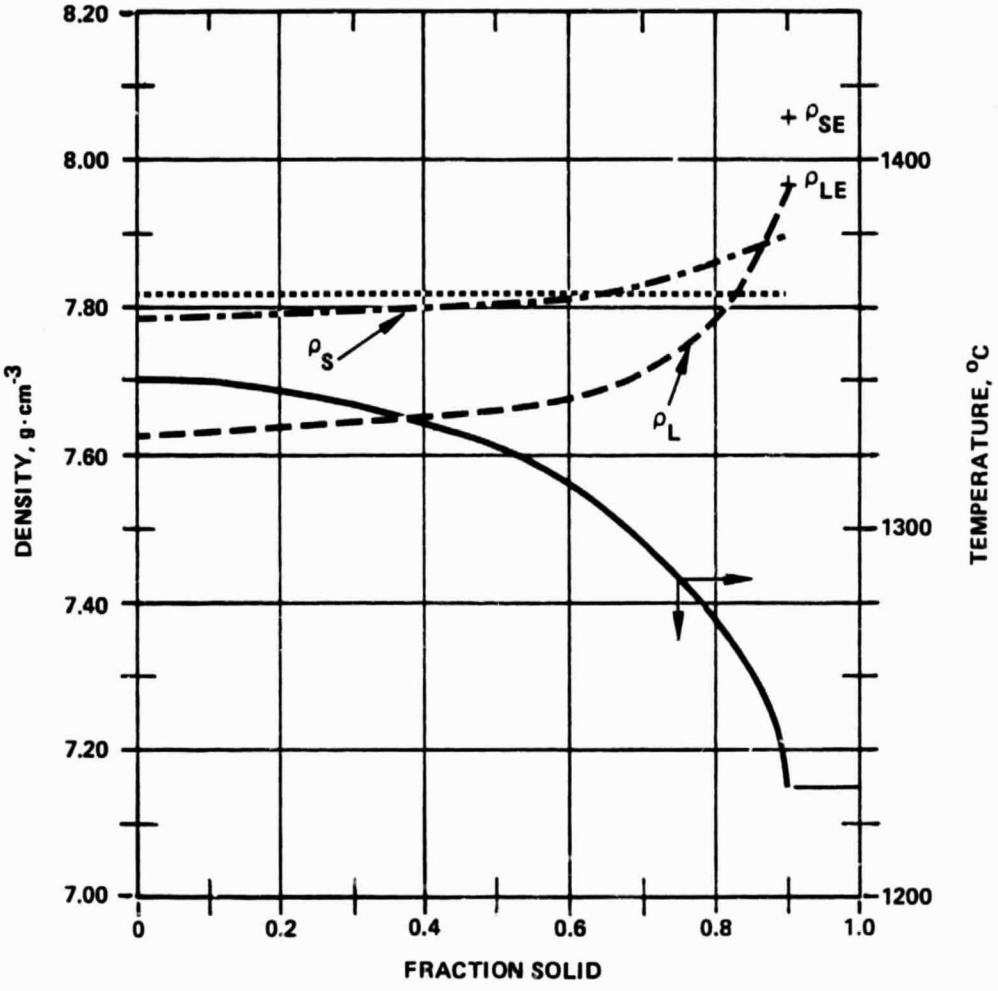

Figure A.1. Densities of Liquid- and Solid-Phases and Fraction Solid During Solidification of MAR-M246(Hf)

APPENDIX B

DATA FOR PWA 1480 (ALLOY 454)

B.1 NOMINAL COMPOSITION

Element	wt. pct.
Cr	10.0
Co	5.0
W	4.0
Ti	1.5
Ta	12.0
Al	5.0

B.2 PARTITION RATIOS

Element	Ratio, k	Source
Cr	0.9	Sellamuthu (6) in MAR-M200
Co	1.1	Jeanfils et al. (8) in Waspalloy
W	1.2	Sellamuthu (6) in MAR-M200
Ti	0.55	Sellamuthu (6) in MAR-M200
Ta	0.70	Kadalbal et al. (14) in Ni-Al-Ta
Al	0.95	Kadalbal et al. (14) in Ni-Al-Ta

B.3 TEMPERATURE DURING SOLIDIFICATION

The temperature during solidification is assumed to vary linearly with composition and temperature according to Eq. (A.1) and the coefficients of Section A.2 apply. A reference temperature of 1412°C for Ni-5.81 wt. pct. Al - 15.18 wt. pct. Ta is used (14). The resulting equation is:

$$T = 1412 - 2.2\, C_{Cr} - 3.2\, (C_{Al} - 5.81) - 7.7\, C_{Ti} + 3.5\, C_{W} - 2.5\, (C_{Ta} - 15.18) \qquad (B.1)$$

Equation (B.1) gives a liquidus temperature of 1403°C and applies to 1290°C when eutectic solidification occurs. The latter temperature was selected because Gell et al. (15) reported that incipient melting in Alloy 454 occurs at 1288°C.

B.4 DENSITY OF THE LIQUID

It is assumed that Eq. (A.3) applies; so that for no molybdenum, carbon, niobium, and hafnium, the density of the interdendritic liquid is

$$\rho_L = 7.66 - 0.013\,(C_{Cr} - 8.08) + 0.001\,(C_{Co} - 9.31) - 0.11\,(C_{Al} - 4.85) - 0.035\,(C_{Ti} - 1.88) + 0.042\,(C_W - 12.76) + 0.035\,C_{Ta} - 0.00125\,(T - 1392) \quad \text{(B.2)}$$

B.5 DENSITY OF THE SOLID

Equation (A.4) and the coefficients listed in Section A.5 are used for PWA 1480. The densities of γ at the elevated temperatures were calculated by calculating compositions for Scheil-type solidification with the partition ratios of Section B.2 and then by using the expansion coefficients in the previous report (3).

Because PWA 1480 contains no carbide, the eutectic comprises $\gamma - \gamma'$ and a small amount of $\gamma - \gamma' - \delta$ which solidifies over a small temperature range (14). As discussed in Section B.4, the solidification of the eutectic is presumed to be isothermal and at 1290°C.

B.6 SUMMARY OF DENSITIES

Figure B.1 summarizes the calculated densities of the liquid- and solid-phases during solidif cation as well as the temperature versus fraction solid.

For convection and macrosegregation calculations, Eqs. (B.1) and (B.2) should be used to calculate the density of the liquid during solidification. For the primary solid-phase, $\rho_s = 7.77\ g \cdot cm^{-3}$ and $\rho_{SE} = 7.86\ g \cdot cm^{-3}$.

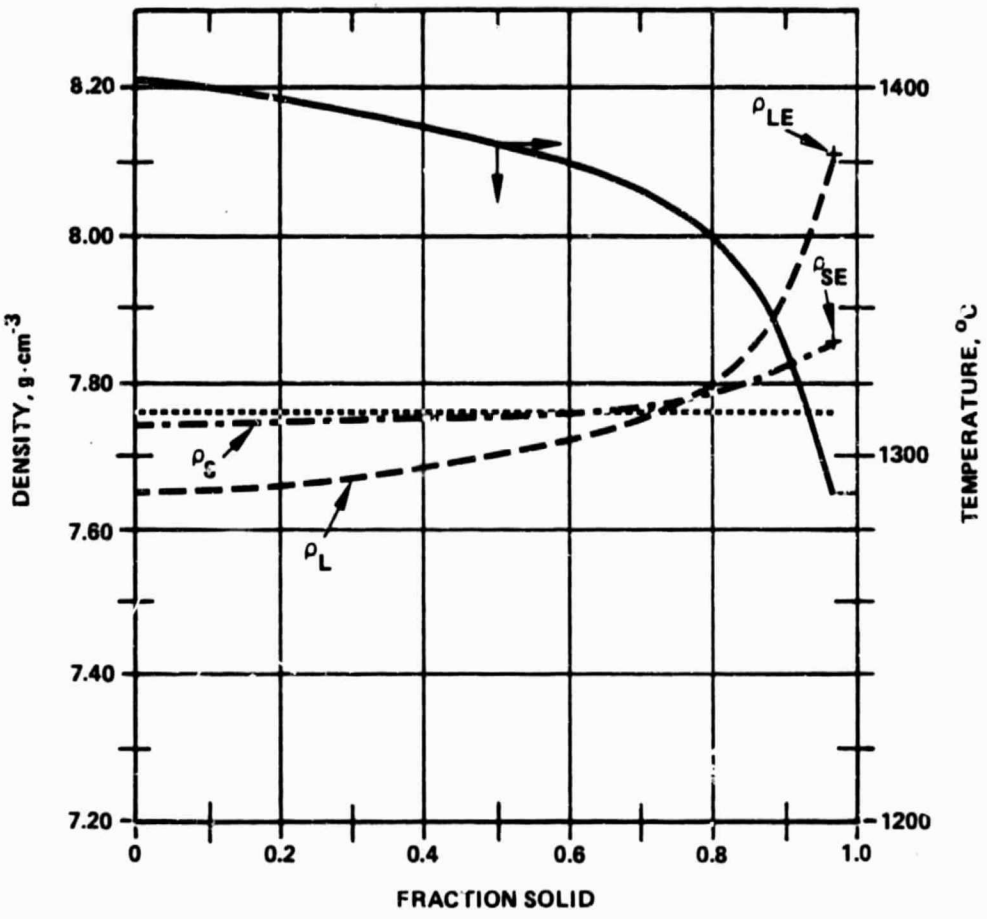

Figure B.1. Densities of Liquid- and Solid-Phases and Fraction Solid During Solidification of PWA 1480 (Alloy 454)

APPENDIX C

FORMATION OF POROSITY IN NICKEL-BASE ALLOYS

During solidification, hydrogen segregates to the interdendritic liquid and, if porosity forms, reacts according to

$$\tfrac{1}{2}H_2\ (g) = \underline{H}. \qquad (C.1)$$

in which $\underline{H}$ indicates that hydrogen is dissolved.

Similar reactions can be written for nitrogen and for oxygen, but the partial pressures of these two elements are negligible when compared to the partial pressure of hydrogen. In the case of nitrogen, almost all of the alloy elements in nickel-base superalloys have the effect of strongly reducing the activity of nitrogen (so that the partial pressure of nitrogen is negligible) and/or the effect of forming nitride compounds. Similarly, the reactive elements in nickel-base superalloys combine with the oxygen to form oxides.

In steel, it is well known that carbon can react with oxygen to form carbon monoxide during solidification:

$$\underline{C} + \underline{O} = CO(g). \qquad (C.2)$$

However, in the presence of strong "deoxidizers," reaction (C.2) does not occur in steel. The reactive elements in nickel-base superalloys, in this regard, are strong "deoxidizers" so that the evolution of carbon monoxide during solidification does not occur.

The free energy of reaction (C.1) in liquid nickel is (16)

$$\Delta G^\circ = 4800 + 8.36T \qquad (C.3)$$

in which the standard state for dissolved hydrogen is taken to be 1 wt. pct. Because

$$\Delta G^\circ = -RT \ln a_H / P_{H_2}^{\frac{1}{2}} \qquad (C.4)$$

then

$$P_{H_2} = a_H^2 \exp\ (8.415 + 4831/T) \qquad (C.5)$$

where

p_{H_2} = partial pressure of hydrogen, atm.

T = temperature, K

R = gas constant, 1.987 cal(gm - atom)$^{-1}$ K^{-1}

and

a_H = activity of hydrogen dissolved in the liquid nickel.

The activity of hydrogen is

$$a_H = f_H C_H \tag{C.6}$$

in which f_H is the activity coefficient of hydrogen and C_H is the concentration of hydrogen in wt. pct. In multicomponent superalloys, the activity coefficient is not known so we resort to a technique, which is strictly applicable to dilute alloys, to estimate f_H. The alloy elements affect f_H according to

$$\log f_H = \sum_j^n e_H^j C_j \tag{C.7}$$

in which e_H^j are the interaction coefficients of each n alloy element.

Sigworth et al. (16) have summarized many values of e_H^j, some of which are given below.

Element	e_H^j	Element	e_H^j
Al	0.014	Ti	0.013
Co	0.0031	Ta	0.011
Cr	0.0036	Hf	0.011
Mo	0.011	C	0.065
W	0.011		

Sigworth et al. (16) presented no data for Ti, Ta, and Hf, so estimates were made based upon the proximity of these elements to others, for which e_H^j is known, in the periodic table. The value for carbon (i.e., e_H^c) is assumed to be that for e_H^c in liquid iron (17).

The partitioning of hydrogen between the liquid- and solid-phases in nickel-base superalloys is not known, but some data are available for nickel, nickel-cobalt alloys, and nickel-iron alloys (18). To extrapolate these data to obtain values of partition ratios, solubility data were plotted as

$\ell n\ s$ vs. $1/T$ as indicated in Fig. C.1 where s is the solubility of hydrogen in equilibrium with 1 atm. of $H_2(g)$. A linear relationship is expected provided ΔG^o is of the form given in Eq. (C.3) and the activity coefficient is independent of temperature.

From Fig. C.1, the partition ratio for hydrogen was determined at 1200°C, 1300°C, and 1400°C for nickel and Ni-20 wt. pct. Fe and at 1400°C for Ni-20 wt. pct. Co. Values ranged from 0.42 to 0.46. A value of $k_H = 0.44$ is recommended.

Sample calculations were done for hydrogen dissolved in PWA 1480 with the properties given in Appendix B. The substitutional alloy elements (Cr, Co, W, Ti, Ta, and Al) were assumed to partition according to Scheil-type solidification and dissolved hydrogen was assumed to partition with uniform concentrations within both phases.

The scheme employed for the calculations follows:

1. Calculate the composition of the interdendritic liquid;
2. Calculate the activity of dissolved hydrogen in the interdendritic liquid with Eqs (C.7) and (C.6); and
3. Calculate the partial pressure of $H_2(g)$ with Eq. (C.5).

Results of such calculations are shown in Fig. C.2. With a melt containing 5 ppm of dissolved hydrogen, the pressure generated is less than 1 atm. until near the end of solidification whereas with 8 and 10 ppm, the pressure generated is substantially greater. Presumably, increasing amounts of microporosity would be expected in, the order of, melts containing 5, 8, and 10 ppm.

To nucleate a gas bubble within the interdendritic liquid, the internal hydrogen pressure must overcome the local pressure within the solid-liquid region and the added pressure due to surface tension.

Specifically,

$$p_{H_2} \geq p + 2\gamma/R \qquad (C.8)$$

where

p_{H_2} = pressure inside the bubble,

p = local pressure,

γ = surface tension, and

R = radius of gas bubble.

For nickel, $\gamma = 1778\ mN \cdot m^{-1}$ (19). As an example, assume that $p = 1$ atm ($1.013\ N \cdot m^{-2}$) and $p_{H_2} = 1.2$ atm ($1.216\ N \cdot m^{-2}$). From Eq. (C.8), it follows that a bubble is stable provided $R \geq 1.65 \times 10^{-4}$ m or 165 μm. A typical primary dendrite arm spacing in directionally solidified superalloys is 300 μm; so, presumably this calculation indicates that microporosity would form.

The use of Eq. (C.8) gives an overestimate of p_{H_2} required to produce a stable bubble because there is no account of the presence of the solid-liquid interface that would provide an active site for bubble nucleation.

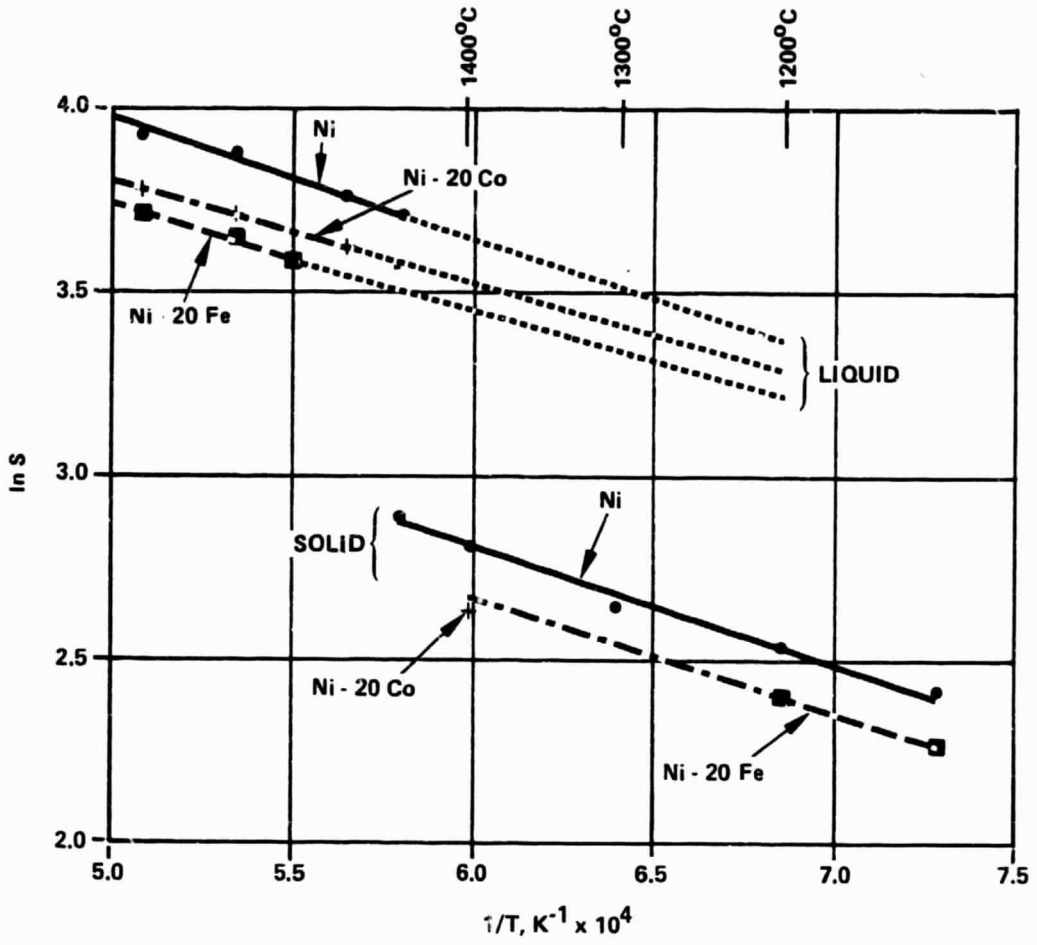

NOTE: Solubility (S) has units of cm^3 of $H_2(g)$ at STP/100 g of metal.

Figure C.1. Solubility of Hydrogen in Nickel and Ni-20 wt. pct. Co and Ni-20 wt. pct. Fe Alloys

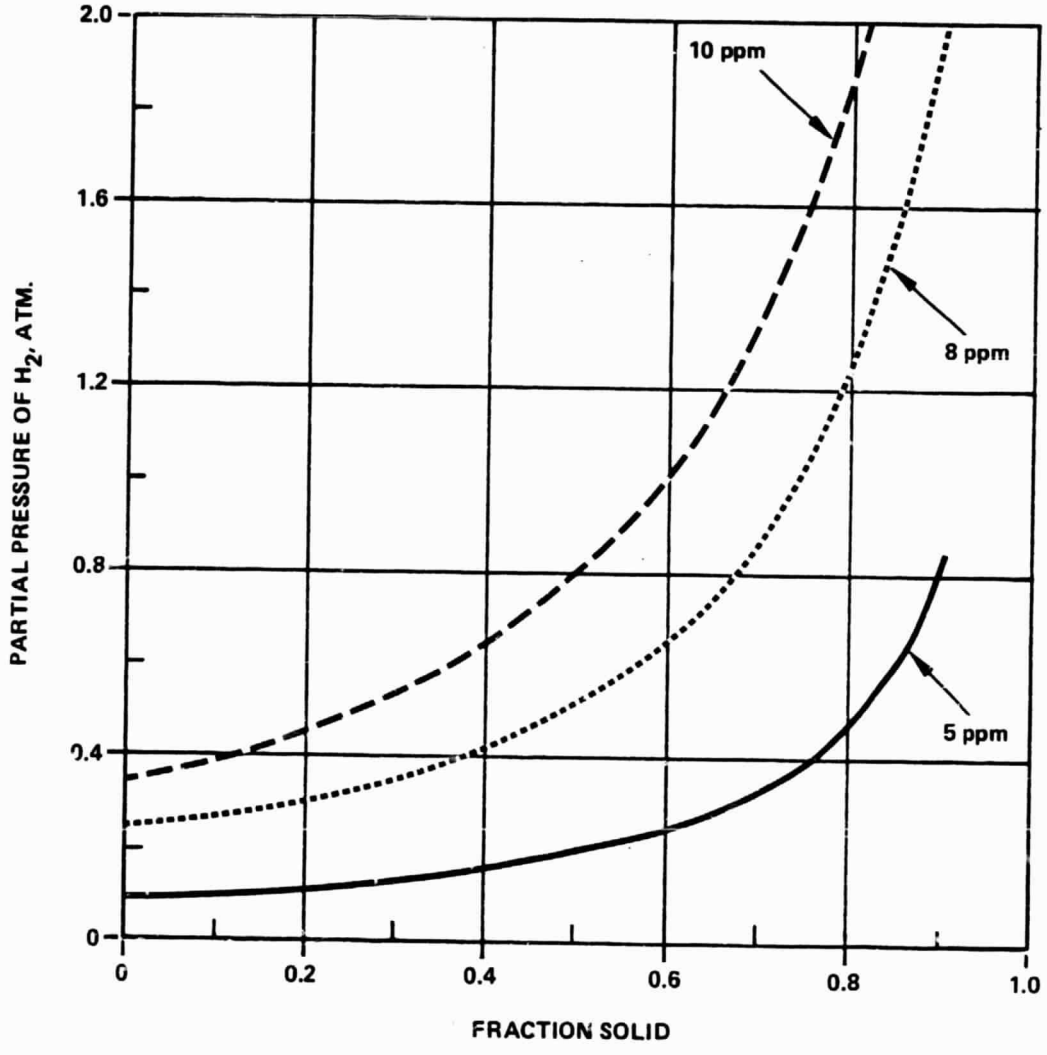

NOTE: Numbers on the curves refer to the concentration of dissolved hydrogen in the melt.

Figure C.2. Partial Pressure of H_2(g) Generated in Interdendritic Liquid During Solidification of PWA 1480

APPENDIX D

SURFACE TENSION IN NICKEL-BASE ALLOYS

A relation derived by Guggenheim (20) for ideal binary solutions was applied by Speiser and Spretnak (21) to estimate the surface excess at a grain boundary; the relation is

$$\exp(-\gamma s/\kappa T) = N_1 \exp(-\gamma_1 s/\kappa T) + N_2 \exp(-\gamma_2 s/\kappa T) \qquad (D.1)$$

where

γ = surface tension,
s = surface area per atom,
T = absolute temperature,
κ = Boltzmann's constant, and
N_1, N_2 = atom fractions.

Speiser (22) has suggested that, lacking data, Eq. (D.1) could be applied to a multicomponent alloy, and it would be better to account for the individual atomic surface areas of each component. Then Eq. (D.1) becomes

$$\exp(-\gamma s/\kappa T) = \sum_i N_i \exp(-\gamma_i s_i/\kappa T) \qquad (D.2)$$

where s_i is the surface area per atom, and s is the weighted average (based upon the atom fractions of all components).

The surface tension of each component is given by

$$\gamma = \gamma_o + (T-T_o)\,(d\gamma/dT) \qquad (D.3)$$

where γ_o is the surface tension of the component at its melting point T_o.

Equations (D.2) and (D.3), together, can be used to calculate the surface tension of the interdendritic liquid during solidification; the calculation accounts for the change in composition and temperature of the interdendritic liquid. Using the data and relations in Appendix A and Appendix B, the composition and temperature of the interdendritic liquid in MAR-M246(Hf) and PWA 1480 were computed assuming Scheil-type solidification. Then Eqs. (D.2) and (D.3) were used to calculate the surface tensions shown as the two lower curves in Fig. D.1.

The atomic surface areas were computed from the atomic radii given in Brandes (23); surface tensions and values of ($d\gamma/dT$) were also taken from Brandes (19). These data are summarized below for the elements in MAR-M246(Hf) and PWA 1480.

Element	T_o, °C	γ_o, dyn·cm^{-1}	$d\gamma/dT$, dyn·cm^{-1}·C^{-1}	s_i, cm^{2}x10^{16}
Cr	1875	1700	-0.32	5.48
Co	1493	1873	-0.49	3.95
Al	660	914	-0.35	6.42
Ti	1685	1650	-0.26	6.80
W	3377	)	-0.29	6.25
Mo	2607	2250	-0.30	6.15
Ta	2977	2150	-0.25	6.80
C	--	--	--	1.86
Hf	1943	1630	-0.21	7.95
Ni	1454	1778	-0.38	4.90

Carbon does not affect the surface tension of iron (24); it is, likewise, assumed not to affect the surface tension of these alloys except by the small effect when the average value of s for the alloy is computed for use in Eq. (D.2).

Figure D.1 shows that the surface tensions of the interdendritic liquid in MAR-M246(Hf) and PWA 1480 are approximately 5-10 pct. less than the surface tension for pure nickel, curves a and b. Curves a and b show a slight variation in surface tension only because the temperature during solidification varies whereas the curves for PWA 1480 and MAR-M246(Hf) reflect both variations: temperature and composition. Clearly, the effect of composition predominates.

Because the surface tensions of the alloys vary only slightly during solidification, it is recommended that constant values be used to predict the formation of porosity during solidification. For MAR-M246(Hf), the recommended value for the surface tension is 1700 dyn·cm^{-1}. For PWA 1480, it is 1710 dyn·cm^{-1}.

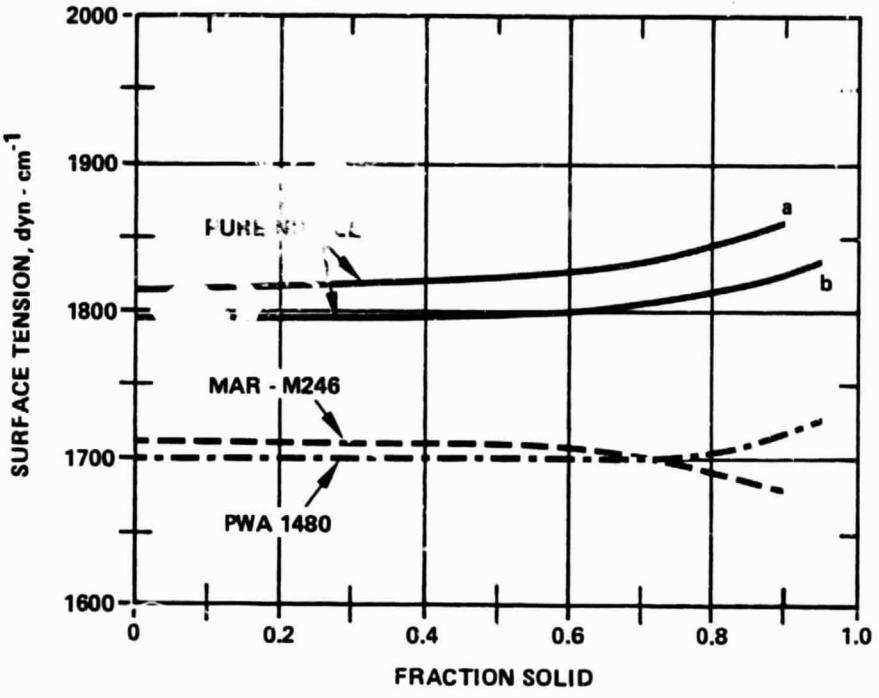

NOTE: Curves a and b show the effect of temperature alone on the surface tension of nickel.

Figure D.1. Surface Tension of Interdendritic Liquid During Solidification of Two Nickel-Base Superalloys

APPENDIX E

FORMATION OF POROSITY IN ALUMINUM-COPPER ALLOYS

The hydrogen reaction during pore formation in aluminum-copper alloys is the same as for pore formation in nickel-base alloys:

$$\tfrac{1}{2}H_2\ (g) = \underline{H}\ , \tag{E.1}$$

in which $\underline{H}$ indicates that hydrogen is dissolved. The expression for the partial pressure of hydrogen is then

$$P_{H_2} = a_H^2 \exp(\ 5.964 + 12508./T\ ) \tag{E.2}$$

where

P_{H_2} = partial pressure of hydrogen, atm.,

T = temperature, K,

and a_H = activity of hydrogen dissolved in the liquid aluminum.

The activity of hydrogen is

$$a_H = f_H\ C_H \tag{E.3}$$

in which f_H is the activity coefficient of hydrogen and C_H is the concentration of hydrogen in weight percent. The effect of copper on the activity coefficient of hydrogen in liquid aluminum is

$$\ln f_H = 0.0748\ C_L - 0.00142\ C_L^2 \text{ at } 750^oC, \text{ and} \tag{E.4}$$

$$\ln f_H = 0.0534\ C_L - 0.000848\ C_L^2 \text{ at } 950^oC, \tag{E.5}$$

where C_L is the weight percent copper in the fluid. To obtain the activity coefficient at temperatures in the solidification range, 548°C to 660°C, Eq. (E.4) and (E.5) are extrapolated linearly in the reciprocal of temperature:

$$f_H = A\, C_L + B\, C_L^2 \text{ at } T\ ^oC, \tag{E.6}$$

where
$$A = A_1 + (A_2-A_1)(1/T-1/T_1)/(1/T_2-1/T_1), \tag{E.7}$$

$$B = B_1 + (B_2-B_1)(1/T-1/T_1)/(1/T_2-1/T_1), \tag{E.8}$$

and the subscripts 1 and 2 reference values at 750°C and 950°C, respectively.

The concentration of hydrogen in the interdendritic liquid is given by the lever rule,

$$C_H = C_{HI}/(g_L + k_H g_S), \tag{E.9}$$

where the partition ratio for hydrogen, k_H, is 0.0555 and C_{HI} is the initial weight percent of dissolved hydrogen in the molten metal.

APPENDIX F

SURFACE TENSION IN ALUMINUM-COPPER ALLOYS

The surface tension of the interdendritic liquid during solidification of aluminum-copper alloys can be calculated in the same manner as for nickel-base alloys (Appendix D). The calculation accounts for the effects of variations in composition and temperature of the interdendritic liquid on the surface tension. Surface tension, temperature, and liquid composition of Al-4.5 wt.pct.Cu are shown in Table F.1 as functions of the volume fraction solid for a Scheil solidification calculation.

Table F.1. Scheil Solidification Calculation Results

Volume Fraction Solid	Liquid Composition (wt.pct.)	Temperature (°C)	Surface Tension (dyn/cm)
0.0	4.5	645	949
0.24	5.65	641	958
0.42	7.07	636	969
0.6	9.62	628	987
0.78	15.78	607	1029
0.9	30.34	558	1118

Because the surface tension varies significantly during solidification, it should be written as a function of temperature or composition. In terms of temperature,

$$\sigma = 854.4 + 2.555\ T - 0.003734\ T^2 \qquad (F.1)$$

where σ is in dyn/cm and T is in °C. In terms of composition,

$$\sigma = 915.0 + 7.828\ C_L - 0.03736\ C_L^2 \qquad (F.2)$$

with σ in dyn/cm and C_L in weight percent Cu in the interdendritic liquid.